Supporting Information

Ctenophore-inspired hydrogels for efficient and repeatable underwater specific adhesion to biotic surfaces

Xing Su,[a] Yang Luo,[a] Zhuoling Tian,[b] Zuoying Yuan,[a] Yiming Han,[a] Runfeng Dong,[b] Liang Xu,[b] Yuting Feng,[a] Xiaozhi Liu,[c] and Jianyong Huang*[a]

[a]Department of Mechanics and Engineering Science, Beijng Advanced Innovation Center for Engineering Science and Emerging Technology, College of Engineering, Peking University, Beijing 100871, China

[b]Academy for Advanced Interdisciplinary Studies, Peking University, Beijing 100871, China

[c]Tianjin Key Laboratory of Epigenetics for Organ Development of Premature Infants, Fifth Central Hospital of Tianjin, Tianjin, 300450, China

*Address correspondence to Jianyong Huang, College of Engineering, Peking University, Beijing 100871, P. R. China

Email: jyhuang@pku.edu.cn ; Tel: +86-10-62751879; Fax: +86-10-62753562

Contents

Experimental Sections

Materials

Acrylic acid (AA) with the purity of 99.0% was purchased from Macklin reagent. N,N'-methylene bisacrylamide (BIS) of the ultra-pure grade was supplied from AMRESCO Inc. Ammonium persulfate (APS) with the purity of 98% was provided by Shanghai Titan Scientific in Shanghai. Tannic acid (TA) with a purity level of PT was bought from Alfa Aesar. Chitosan (CHI) with a molecular weight of 50,000-190,000 Da based on viscosity, and the degree of deacetylation of 75-85% was bought from Sigma Aldrich. $Al(NO_3)_3{\cdot}9H_2O$, Sodium hydroxide (NaOH) and hydrochloric acid (HCl, 37 wt%) with the purity level of AR were supplied by Beijing Tong Guang Fine Chemicals Company. 75% ethanol was supplied by Shandong ANNJET high tech Disinfection Technology Co. Ltd. All chemicals, solvents and other consumable materials were purchased and used as received, unless specially noted.

Synthesis of gels

The designed amount of TA (0 g, 0.1 g, 0.2 g or 0.3 g), CHI (0 g, 0.1 g, 0.2 g or 0.3 g) and $Al(NO_3)_3{\cdot}9H_2O$ (0 g, 0.04 g, 0.06 g, 0.08 g or 0.1 g) were added and dispersed into 10 g of deionised water under constant stirring. Next, 3 g AA and 10 mg BIS were added and the mixture was stirred for 20 min to reach complete dissolution. Finally, 0.08 g APS was dissolved in a designed amount of distilled water, and then being added into the mixture drop by drop under stirring. The obtained solution was treated by ultrasonication for removing the bubbles and sealed in the plastic moulds. The polymerization was conducted in the water bath starting at 60 ^{o}C. The temperature was then gradually enhanced to 80 ^{o}C in 30 min and kept at 80 ^{o}C for another 30 min.[1] The detailed compositions and abbreviations of the samples synthesised in this study were listed in the **Table S1**. The cylindrical moulds with the inner diameter of 3 mm were used for preparing samples for the subsequent tests unless otherwise noted.

Characterisations

Fourier transform infrared (FTIR) spectroscopy was conducted on a PerkinElmer Spectrum 100 spectrophotometer. Each spectrum was measured by 16 scans in a wavenumber range from 4000 to 600 cm^{-1} at the resolution of 1 cm^{-1}. Scanning electron microscopy (SEM) was carried out on a TESCAN MAIA3 ultra high-resolution field emission scanning electron microscope (acceleration voltage: 5 kV). The fractured surfaces of the freeze-dried hydrogel samples were coated with gold and observed. Rheological tests were carried out on an AR-G2 Advanced Rheometer (TA Instruments). The storage moduli G' and loss moduli G" of the

samples containing different amount of CHI (P-0.08Al-0.3TA, P-0.08Al-0.1C-0.3TA, P-0.08Al-0.2C-0.3TA & P-0.08Al-0.3C-0.3TA) were measured by the dynamic frequency sweeps in the range of the angular frequency from 0.1 to 10 $rads^{-1}$ at ambient temperature. A fixed strain of 1% was chosen via strain sweep tests, confirming it was in the linear viscoelastic region. A parallel plate geometry with a diameter of 20 mm and a gap of 1.0 mm between two parallel plates was used. The swelling tests of the hydrogels were operated by emerging the cylindrical freeze-dried hydrogel samples with the length of 5 mm and the diameter of 3 mm in excess distilled water or PBS. After two weeks, the samples were weighed and the swelling ratios were calculated by the equation: $SR = (W_s - W_d)/W_d$, where W_d and W_s were the weight of the samples before and after swelling, respectively. For each material, 5 specimens were tested. The electrical tests were conducted as follows: A P-0.08Al-0.3C-0.3T hydrogel strip was adhered onto author's index finger covered with latex glove and then connected to electrodes. The finger bent cyclically at the bending angle of 0º, 45º and 90º. The electrical signals of the deformed hydrogel were measured by using a CHI760E electrochemical workstation (CH instruments Ins.). The relative change of the resistance is calculated by the equation: $\Delta R/R_0$ / % = $(R-R_0)/R_0$ / %, where R_0 and R represented the resistance without and with the corresponding bending deformation, respectively.

Mechanical testing

The tensile tests were carried out on a STS10N tensometer (Xiamen East Instrument Co. Ltd.) equipped with a 10 N load cell, at the crosshead speed of 100 mm min^{-1}. The tested cylindrical samples were 15 mm long, and with a gauge length of 5 mm. For the cyclic tensile tests, a maximum strain of 5 was chosen. The adhesive tests were conducted on the same tensometer. Two pieces of substrates were stick together by the hydrogel (**Fig. 3a**) with the bonding area of 10×10 mm^2, pressed by finger (pressure ~ 1 kPa) for 10 sec in air or underwater at ambient temperature without any additional treatment, and then the external pressure was removed immediately.[2] Undergoing different bonding time (10 sec, 5 min, 10 min, 30 min, 180 min or 1440 min) in air or underwater, without any external pressure or post-treatment, the adhered substrates were submitted to a shear stress when applied to the tensometer, at a crosshead speed of 5 mm min^{-1} (lap-shear tests, see **Fig. S13**).[2] The maximum stress during shear adhesive tests were recorded as the adhesive strength, calculated by the maximum force divided by the initial bonding area. Normal smooth, untreated soda-lime glass and high-carbon steel were used as abiotic substrates. Some glass slices were immersed in piranha solution for 2 hours, bringing in enriched surface hydroxyl groups.[3] Some other glass slices were polished

by sand paper with 80 M (mesh number) or 320 M for achieving different surface roughness. It was worth noticing that if there was no special explanation, "glass" appeared in this work represented the normal untreated glass. Without any post-treatment such as degreasing[4] or surface liquid removal,[2, 5] different fresh and untreated tissues including porcine skin, liver, muscle and intestines were also tested. Repeated (1~30 times) adhesions were performed and studied. Porcine skin samples were adhered in an aquatic environment at different pH (4, 6, 8 or 9), or with different solutes (urea, glycine, uric acid, glucose or cholesterol) and the corresponding adhesive properties were investigated. Different post-treatment for the underwater of porcine skins by medical ethanol, alkali or acid were taken into consideration. For each mechanical test, at least 8 samples were tested for achieving the statistical data.

Cytocompatibility testing

Cytocompatibility in vitro was conducted by culturing L929 fibroblast cells (kindly gifted by the group of Prof. Cai Qing, Beijing University of Chemical Technology) with complete RPMI medium 1640 (Giboc) containing 10% fetal bovine serum (Giboc) and 1% penicillin-streptomycin solution (Giboc) in a 5% CO_2 incubator at 37 ^oC,[6] The tested hydrogels were washed with deionized water for 3 days. Afterwards, the residual toxic AA monomers or APS initiators were mostly removed.[5] And then immersed into complete medium to make extracts and sterilized the extracts by 0.2 μm filter. The cells were treated with trypsin-EDTA (Giboc) and resuspended cells with the extracts. The cells with the density of 1×10^3 were seeded into each well (96 -well plate) and allowed to grow for 24 hr, 48 hr and 96 hr. The cytocompatibility of the hydrogels were analysed by cell counting kit-8 (CCK-8) assay (Bimake) and Live/Dead assay. CCK-8 assay was conducted as follows: After a specific period of incubation in 96-well plate, CCK-8 solution was diluted by 10 times with the extracts.[7] After the removal of the original medium, 100 μL CCK-8 reagent were added into each well, which were co-cultured with the cells in a 5% CO_2 incubator at 37 ^oC for 2 hr before measurement of the absorbance with a microplate reader (BIO RAD) at a wavelength of 450 nm. After CCK-8 assay, Live-Dead assay was carried on.[2] 2 μM calcein AM (in DPBS) and 4 μM EthD-1 (Invitrogen) working solution were added into wells. The 96-well plate was then incubated in a 5% CO_2 incubator at 37 ^oC for 20 min. A laser scanning confocal microscope (Nikon, Japan) was used to observe the morphologies of the cells. For each group, 6 parallel experiments were conducted for obtaining the convincing results.

Antibacterial activity

Before performing anti-bacterium tests, all the tested hydrogels were sterilised under UV for 30 min in the clean bench. To analysis the inhibitory zone of the hydrogel, *S. aureus* (ATCC 29213) and *E. coli* (ATCC 25922) were mixed in Mueller-Hinton Agar (MHA) medium with a density of 10^6 CFU/mL, then placed the sterilized hydrogel in the center of the flat. After cultured in 37 ℃ for 24 hr, measured the diameters of inhibitory zone by Image J. To evaluate the inhibitory efficiency of the hydrogel on *S. aureus* and *E. coli* growth, the sterilized hydrogels were co-cultured with the 10^8 CFU/mL *S. aureus* and *E. coli* in Mueller-Hinton Broth medium for 24 hr, respectively. After diluted the bacterium solution for 10^4 times, coated on the LB agar plate and cultured in 37 ℃ for 24 hr, count the number of clones on the plate by Image J. For each group, 3 parallel experiments were conducted for obtaining the convincing results.

Wound healing

Care and operation of animals followed the international standards on animal welfare and the protocol was approved by the Animal Care and Use Committee of Fifth Central Hospital of Tianjin (Tianjin, 300450, P.R. China). Experimental rats were purchased from Sibeifu (Beijing) Biotechnology Co., Ltd. They were fed with ad libitum access to food and water under a controlled temperature (22-24℃) and stable humidity (40-60%). Four female SD rats (200-250 g) were used to create the incisions (2 cm) on the back of the rats to evaluate wound healing effect. After sterilization, four incisions were made on the back of each rats. In this assay, incisions were treated with PBS (control group), suture closure, P-0.08Al-0.3C hydrogel patch and P-0.08Al-0.3C-0.3T hydrogel patch. The wound healing effect was observed at 1, 3, 5, and 7 days post-operation. The rats were euthanized to harvest the skin tissue containing the wound area 7 days post-operation. Paraffin Sections in 5 μm thickness were prepared for histological analysis which was stained with hematoxylin and eosin (H&E). The mean wound length of epidermis and dermis were calculated using Image J software. All the measurements were blinded to the tested groups. For each group, 4 parallel experiments were conducted for obtaining the convincing results.

Statistical analysis

All quantitative data were shown in the form of mean ± standard deviation (SD). One-way analysis of variance (ANOVA) with Turkey's test was used for statistical analysis. Differences between groups of $p < 0.05$ was regarded as statistically significant. $p < 0.01$ and $p < 0.001$ were realised as highly significant.

Supplementary Figures

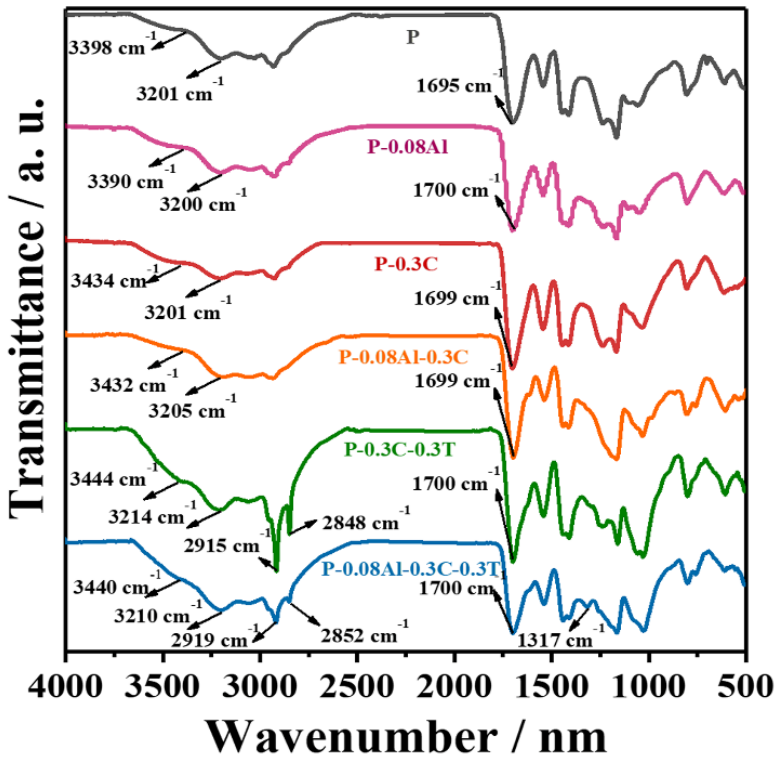

Fig. S1. FTIR spectra of the P, P-0.08Al, P-0.3C, P-0.3C-0.3T, P-0.08Al-0.3C and P-0.08Al-0.3C-0.3T hydrogels.

For P-0.3C-0.3T, the two peaks at 3444 cm^{-1} and 3214 cm^{-1} became higher than those of the hydrogels without TA. This was due to phenol groups of TA, which overlapped with hydroxyl and amine groups.[8] They became sharper and shifted to the left, comparing to those of the hydrogels without TA, indicating that the formation of hydrogen bonds and electrostatic bonds between TA and CHI.[8, 9] Besides, the two peaks at 2848 cm^{-1} and 2915 cm^{-1}, were indicative of carboxyl hydroxyl groups from PAA. Those two sharpened peaks implied the formation of hydrogen bonds between hydroxyl groups of PAA and TA.[10] Similar phenomena were found in the curve of P-0.08Al-0.3C-0.3T. The peak at 1695 cm^{-1} for P was characteristic for carboxyl C=O groups. This peak of other hydrogels underwent a red shift, which resulted from the PAA-Al^{3+} chelation and/or PAA-CHI electrostatic bonds.[11, 12] From P to P-0.3C, the peak at 3434 cm^{-1} moved toward the larger wavenumbers, which confirmed the hydrogen bonds and electrostatic bonds between PAA and CHI.[12] The peak at 1317 cm^{-1} in P-0.08Al-0.3C-0.3T was due to in-plane bending vibration of phenol groups of TA, which was absent in P-0.3C-0.3T. This was indicative of the formation of TA-Al^{3+} chelation.[13]

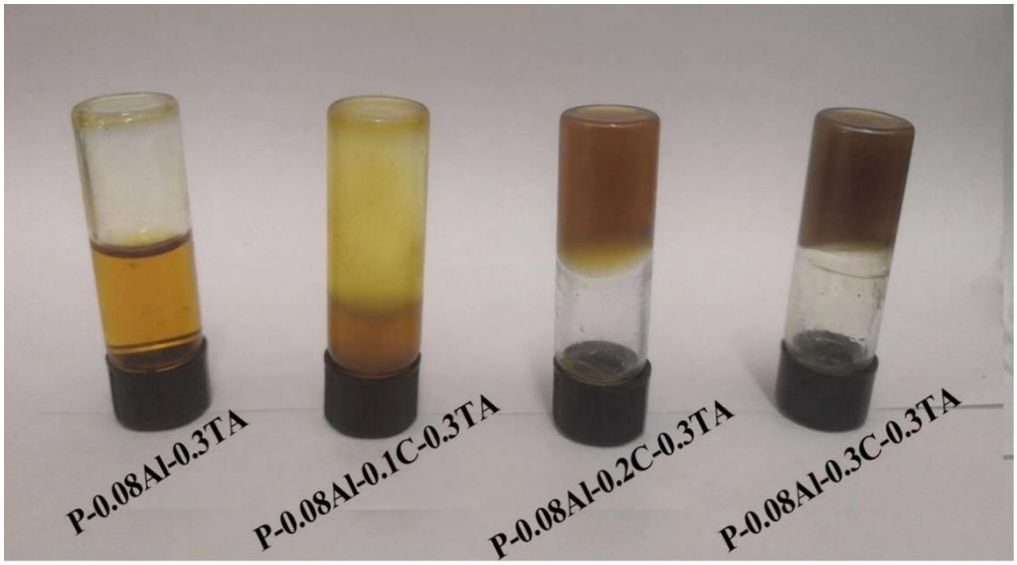

Fig. S2. The impact of different CHI contents on gelation of the TA-containing samples.

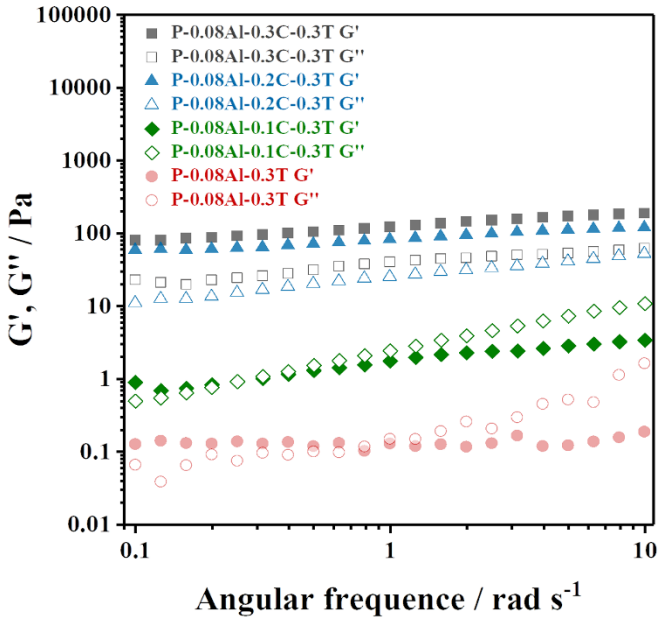

Fig. S3. Rheological data of TA-containing samples with different contents of CHI.

As for the hydrogels containing 0.3 g or 0.2 g CHI, the storage modulus (G′) were apparently larger than the corresponding loss modulus (G′′), which was indicative of elastic soft matters.[1, 14, 15] By contrast, the ones containing 0 g or 0.1 g CHI displayed larger G′′ than G′ when the angular frequency was larger than 1 rad s^{-1}, implying they were lightly crosslinked viscous polymeric solutions and the gelation was incomplete.[5]

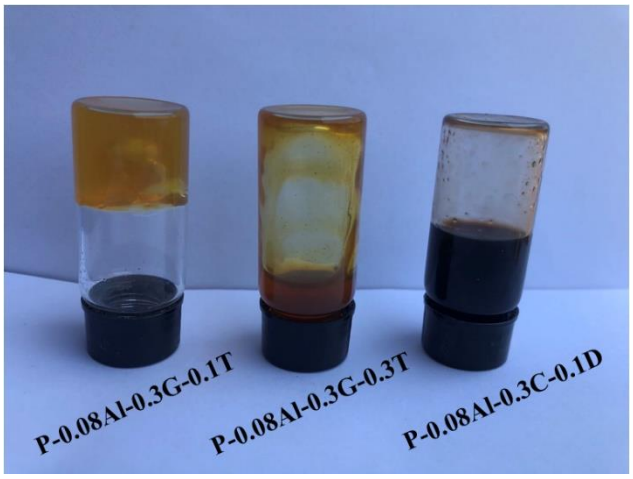

Fig. S4. The polymerised P-0.08Al-0.3G-0.1T, P-0.08Al-0.3G-0.3T and P-0.08Al-0.3C-0.1D samples.

After polymerisation, P-0.08Al-0.3G-0.1TA on the left reached gelation while P-0.08Al-0.3G-0.3TA on the right became viscous liquid. Guar gum was neutralized and interacted with other substances in the hydrogel via hydrogen bonding.[16] As for P-0.08Al-0.3C-0.1D, the acidity of catechol groups for dopamine were quite weak, which interacted with CHI via hydrogen bonding rather than electrostatic bonding.[17] Despite the lower amount of polyphenols, the gelation of P-0.08Al-0.3C-0.1D was significantly inhibited.[5] These results demonstrated that both hydrogen bonding and electrostatic interactions between TA and CHI guaranteed the formation of hydrogels.

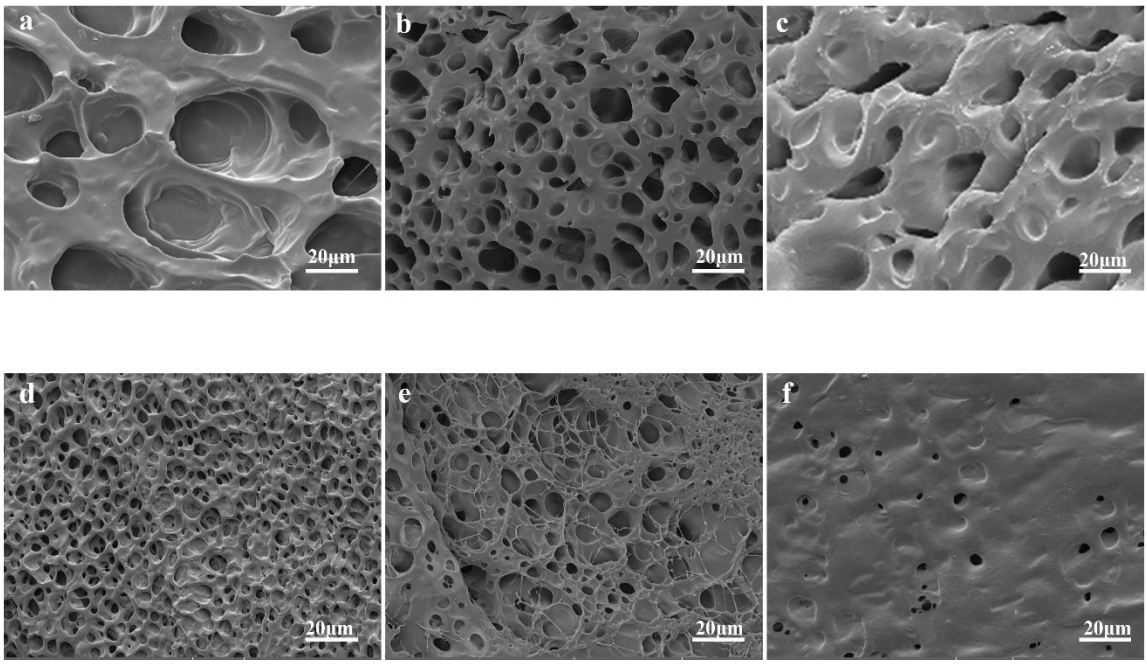

Fig. S5. Scanning electron microscopic graphs of the freeze-dried cross-sectional surfaces of **a** P, **b** P-0.08Al, **c** P-0.3C, **d** P-0.3C-0.3T, **e** P-0.08Al-0.3C and **f** P-0.08Al-0.3C-0.3T hydrogels.

Our further analysis based upon SEM images showed that the fabricated hydrogel (P-0.08Al-0.3C-0.3T) had relatively compact structures in comparison with the control samples that had typical loose porous structures of chemically crosslinked hydrogels. This implied that the greatly increased crosslinking density of P-0.08Al-0.3C-0.3T, comparing to other control samples.[1]

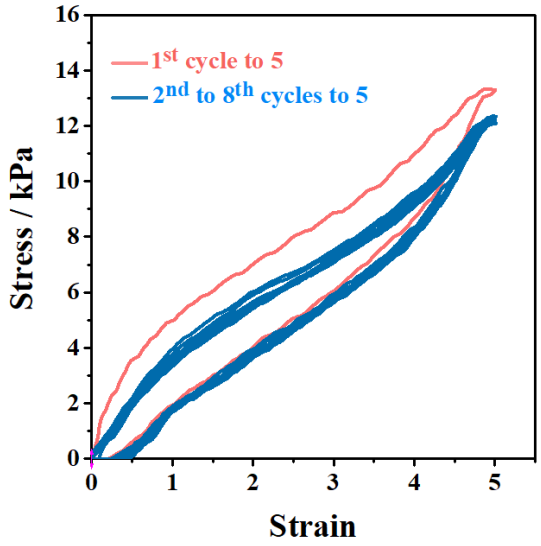

Fig. S6. Cyclic tensile curves of P-0.08Al-0.3C-0.3T to a maximum strain of 5.

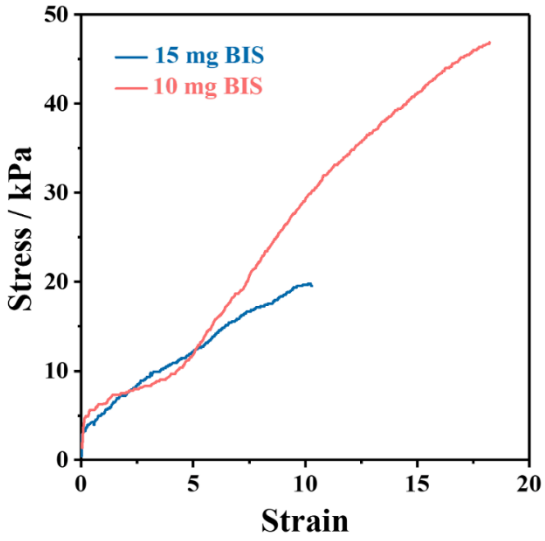

Fig. S7. Tensile curves of P-0.08Al-0.3C-0.3T hydrogels with different contents of BIS.

Lower amount of BIS (5 mg) led to incomplete crosslinking, while higher amount of BIS (15 mg) significantly embrittled the hydrogel.[18, 19]

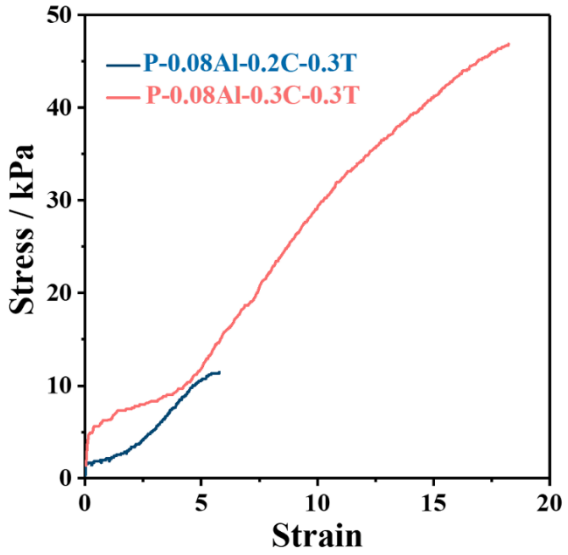

Fig. S8. Tensile curves of hydrogels with different CHI contents.

Lower amount of CHI (0.2 g) brought in drastically reduced mechanical properties mainly because of the reduced hydrogen bonds, electrostatic bonds and chain entanglement donated by CHI.[20]

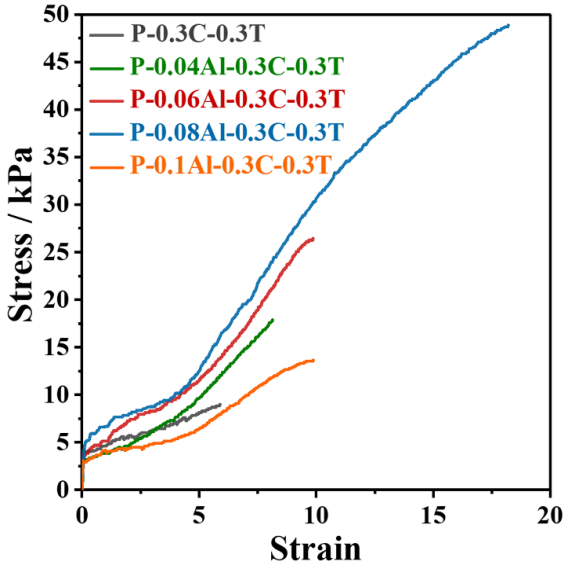

Fig. S9. Tensile curves of hydrogels with different Al^{3+} contents.

P-0.08Al-0.3C-0.3T turned out to be the optimal formula for achieving the best mechanical properties. Lower amount of Al^{3+} made inadequate PAA-Al^{3+} and TA-Al^{3+} ionic crosslinks in adsorbing tensile energy.[18] While higher amount of Al^{3+} could interrupt PAA-CHI electrostatic interactions and thus decreased the mechanical properties.[21]

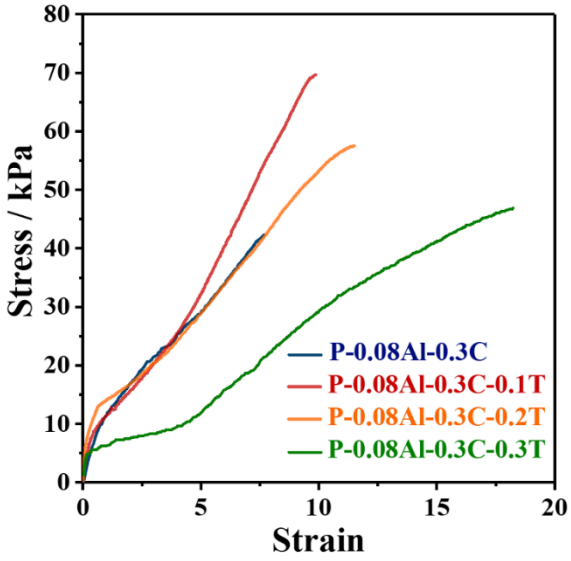

Fig. S10. Tensile curves of hydrogels with different TA contents.

With increasing TA content from 0.1 g to 0.3 g, the tensile strength of the samples took on a decreasing trend whereas the corresponding strain at break increased, which was in accordance with some previously reported hydrogels based on polyphenols.[5, 22] It was inferred that a large number of weak interactions by TA formed a large number of reversible bonds with the hydrogel networks. They significantly reduced the rigidity of hydrogels and thus made them softer and more ductile.[5, 18, 22]

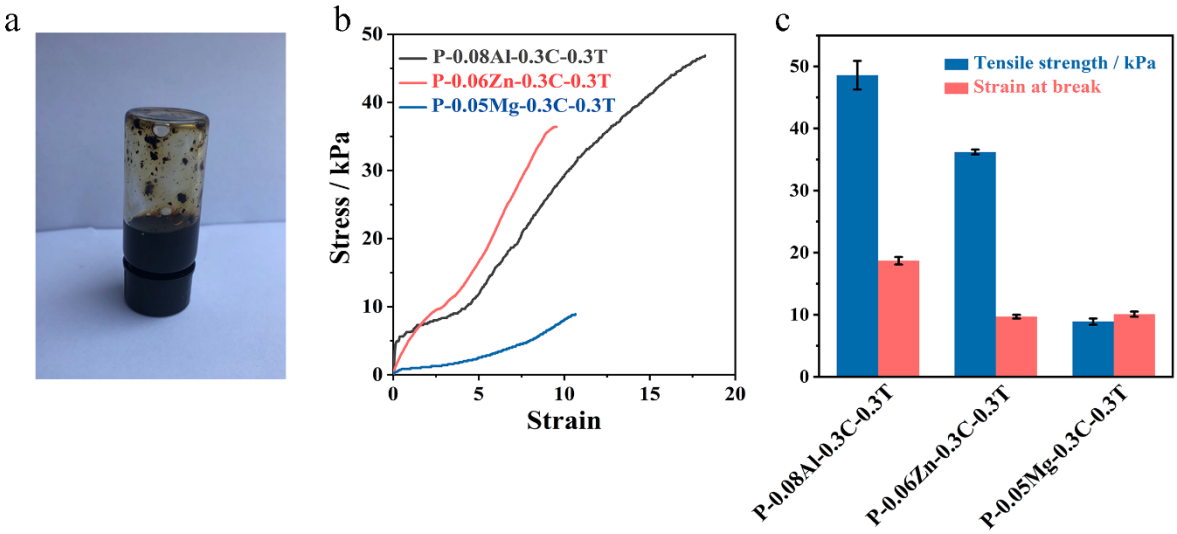

Fig. S11. Al^{3+} in P-0.08Al-0.3C-0.3T was replaced by the equimolar Fe^{3+}, Zn^{2+} and Mg^{2+}, making P-0.08Fe-0.3C-0.3T, P-0.06Zn-0.3C-0.3T and P-0.05Mg-0.3C-0.3T hydrogels, respectively. **a** TA-Fe precipitates appeared and the gelation of P-0.08Fe-0.3C-0.3T failed. **b** The representative tensile curves of P-0.08Al-0.3C-0.3T, P-0.06Zn-0.3C-0.3T and P-0.05Mg-0.3C-0.3T. **c** Statistical data of the mechanical properties of P-0.08Al-0.3C-0.3T, P-0.06Zn-0.3C-0.3T and P-0.05Mg-0.3C-0.3T.

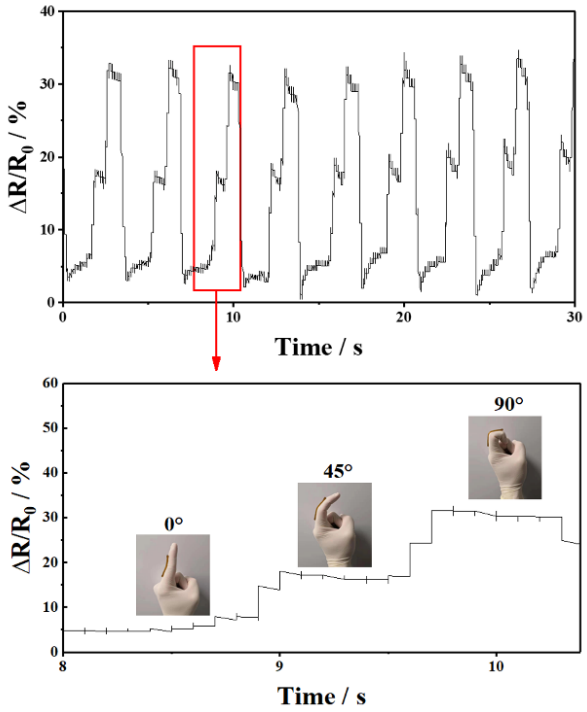

Fig. S12. Demonstration of the P-0.08Al-0.3C-0.3T hydrogel as wearable sensors for real-time monitoring of various finger motions (finger bending for 0°, 45° and 90°).

The charged PAA, CHI, TA and Al^{3+}, as well as the elastic hydrogel network gave rise to strain-sensitive conductivity of P-0.08Al-0.3C-0.3T.[18]

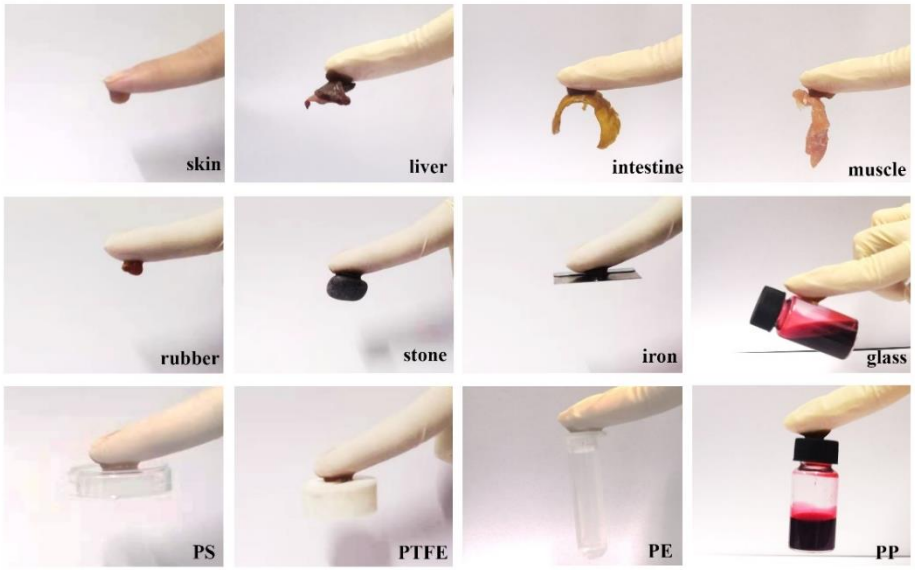

Fig. S13. In-air adhesiveness of P-0.08Al-0.3C-0.3T to various surfaces including: skin, liver, intestine, muscle, rubber, stone, iron, glass, polystyrene, PTFE, polyethylene and polypropylene.

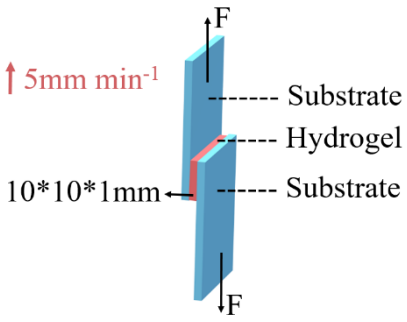

Fig. S14. Schematic illustration of lap-shear tests.

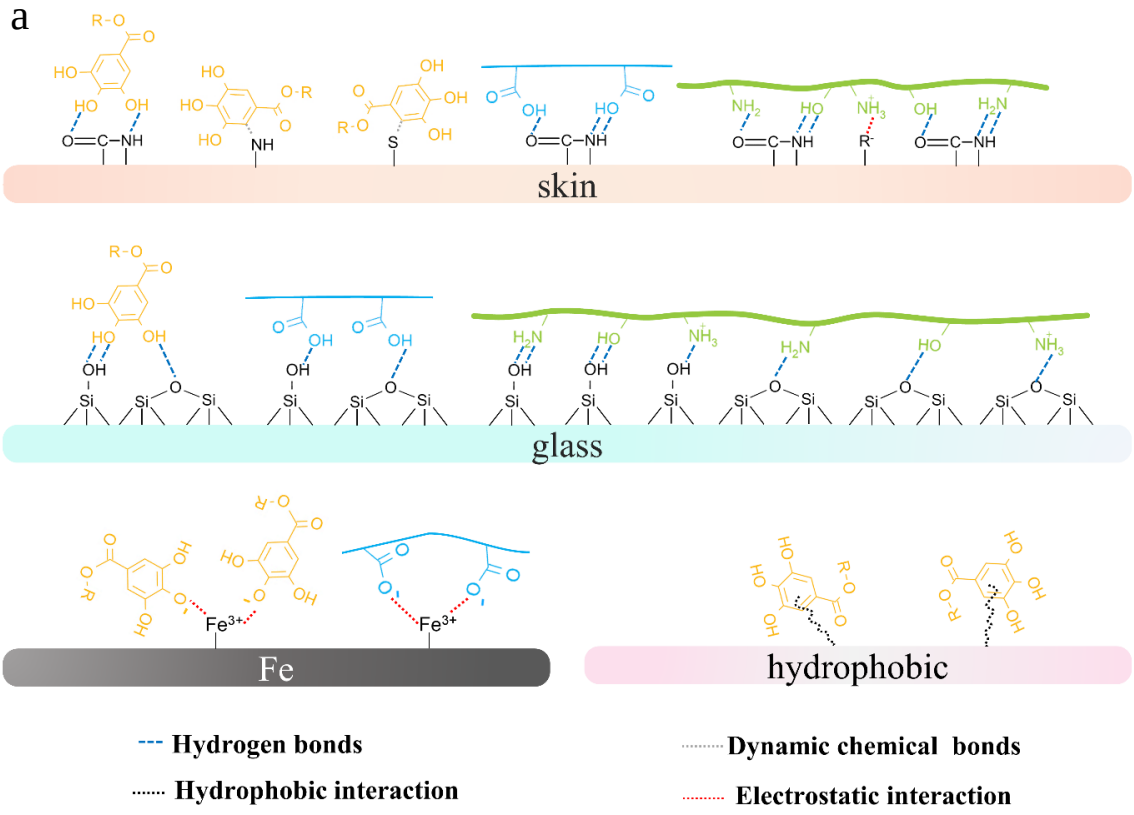

Fig. S15. The adhesive mechanisms of P-0.08Al-0.3C-0.3T to skin, glass, iron and hydrophobic substrates in air.

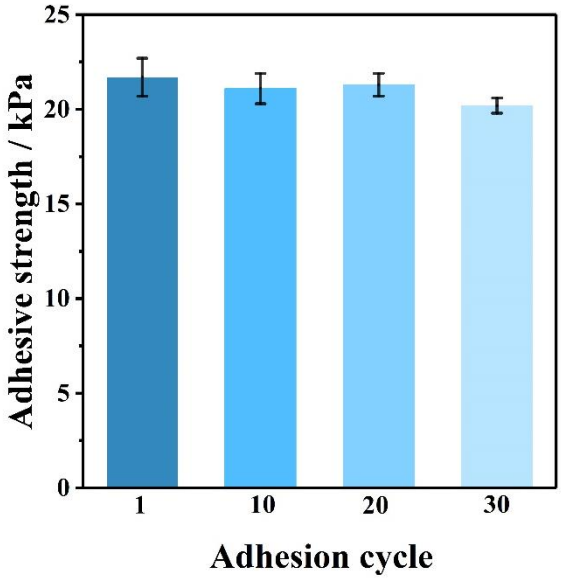

Fig. S16. The in-air adhesive strength of P-0.08Al-0.3C-0.3T to fresh porcine skin after 10, 20, or 30 times of repeated adhesive cycles (Pressed for 10 sec in air, then the pressure was removed and the samples were immediately tested. In air, the adhered samples were peeled off and then adhered again with the same piece of hydrogel for multiple times).

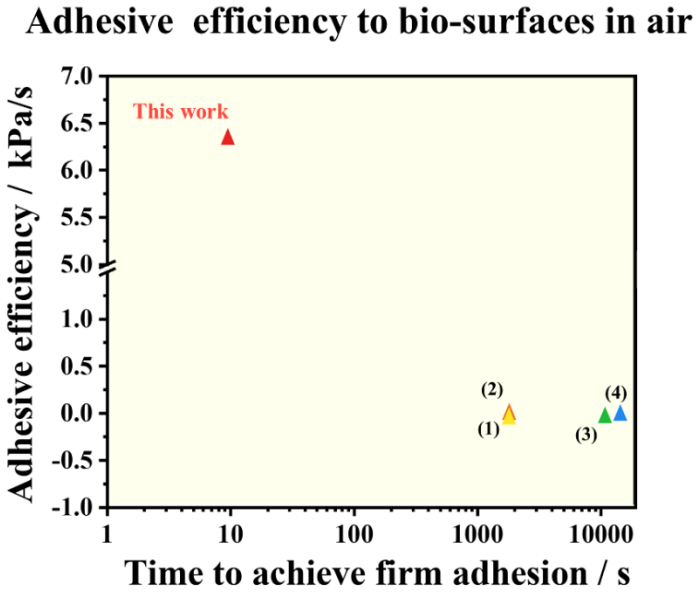

Fig. S17. Review on the adhesive efficiency to porcine skin of the reversibly adhesive hydrogels including (1),[23] (2),[24] (3),[25] and (4).[26] Herein, we defined a concept of adhesive efficiency, which was calculated by the adhesive strength (kPa) divided by the corresponding time (in second) needed for firm adhesion.

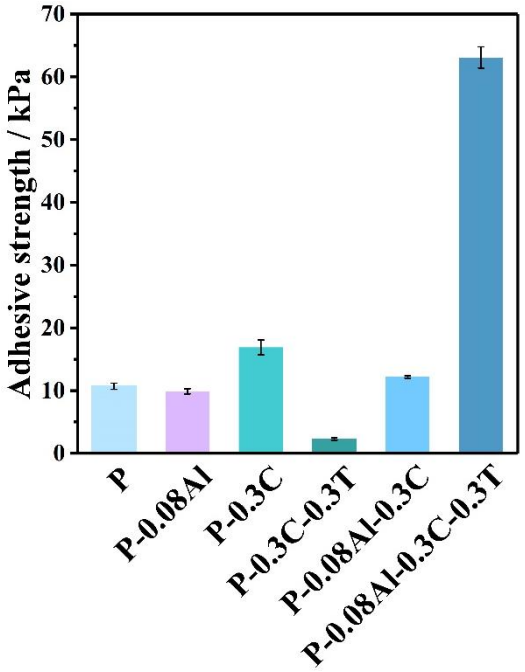

Fig. S18. Adhesive strength of the P, P-0.08Al, P-0.3C, P-0.3C-0.3T, P-0.08Al-0.3C and P-0.08Al-0.3C-0.3T hydrogels to fresh porcine skin (Pressed for 10 sec in air, then the pressure was removed. The samples were left alone in air for 10 min, and then tested).

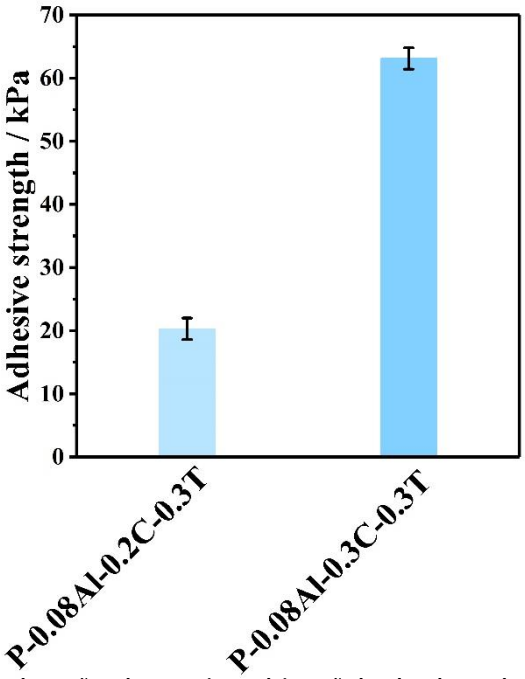

Fig. S19. Adhesive strength to fresh porcine skin of the hydrogels with different contents of CHI (Pressed for 10 sec in air, then the pressure was removed. The samples were left alone in air for 10 min, and then tested). Higher amount of CHI provided more electrostatic bonding sites and improved the adhesive strength.[24, 27]

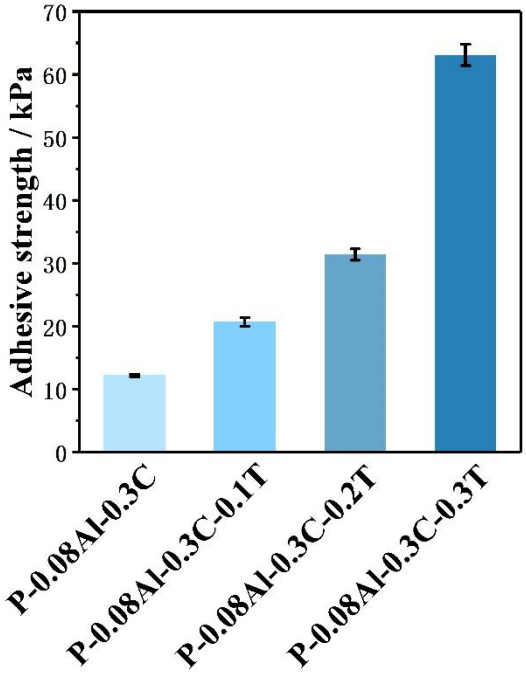

Fig. S20. Adhesive strength to fresh porcine skin of the hydrogels with different contents of TA (Pressed for 10 sec in air, then the pressure was removed. The samples were left alone in air for 10 min, and then tested). Higher amount of TA provided more catechol groups and improved the adhesive strength.[5, 18]

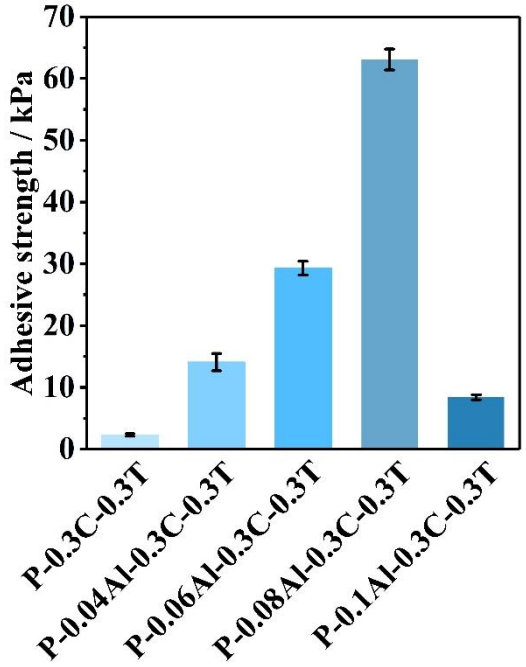

Fig. S21. Adhesive strength to fresh porcine skin of the hydrogels with different contents of Al^{3+} (Pressed for 10 sec in air, then the pressure was removed. The samples were left alone in air for 10 min, and then tested). Al^{3+} could effectively toughen the hydrogel network and thus affect the adhesiveness.[18]

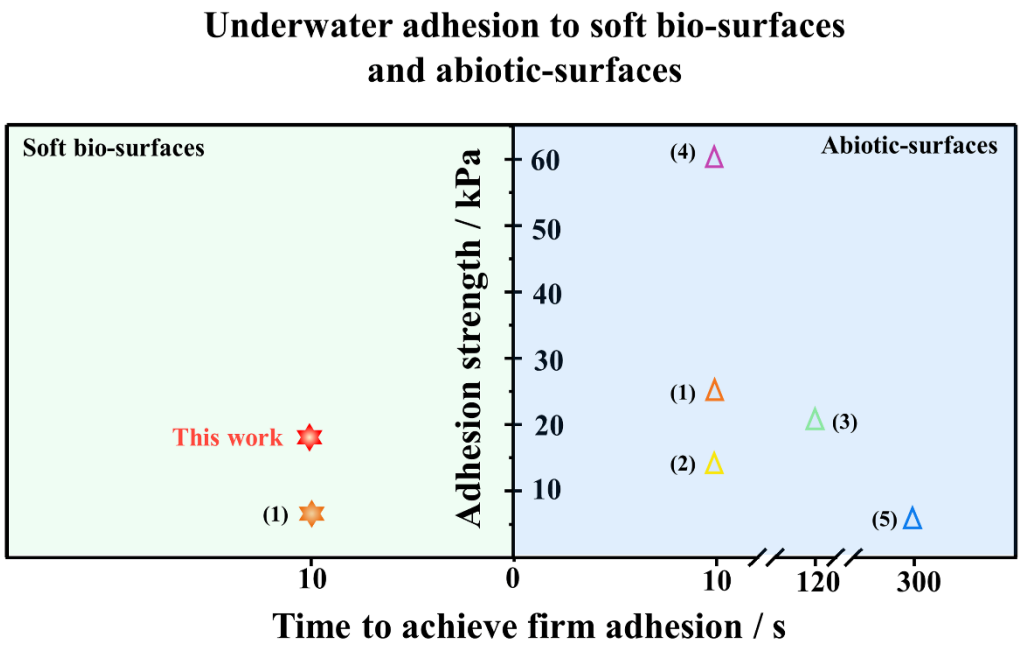

Fig. S22. Review on the underwater adhesion to soft bio-surfaces and abiotic-surfaces of the reversibly adhesive hydrogels including (1) (pork heart)[28] for the soft bio-surfaces, (1) (polyampholytes),[28] (2) (ceramic),[29] (3) (glass),[4] (4) (glass),[30] (5) (hydrogels).[31]

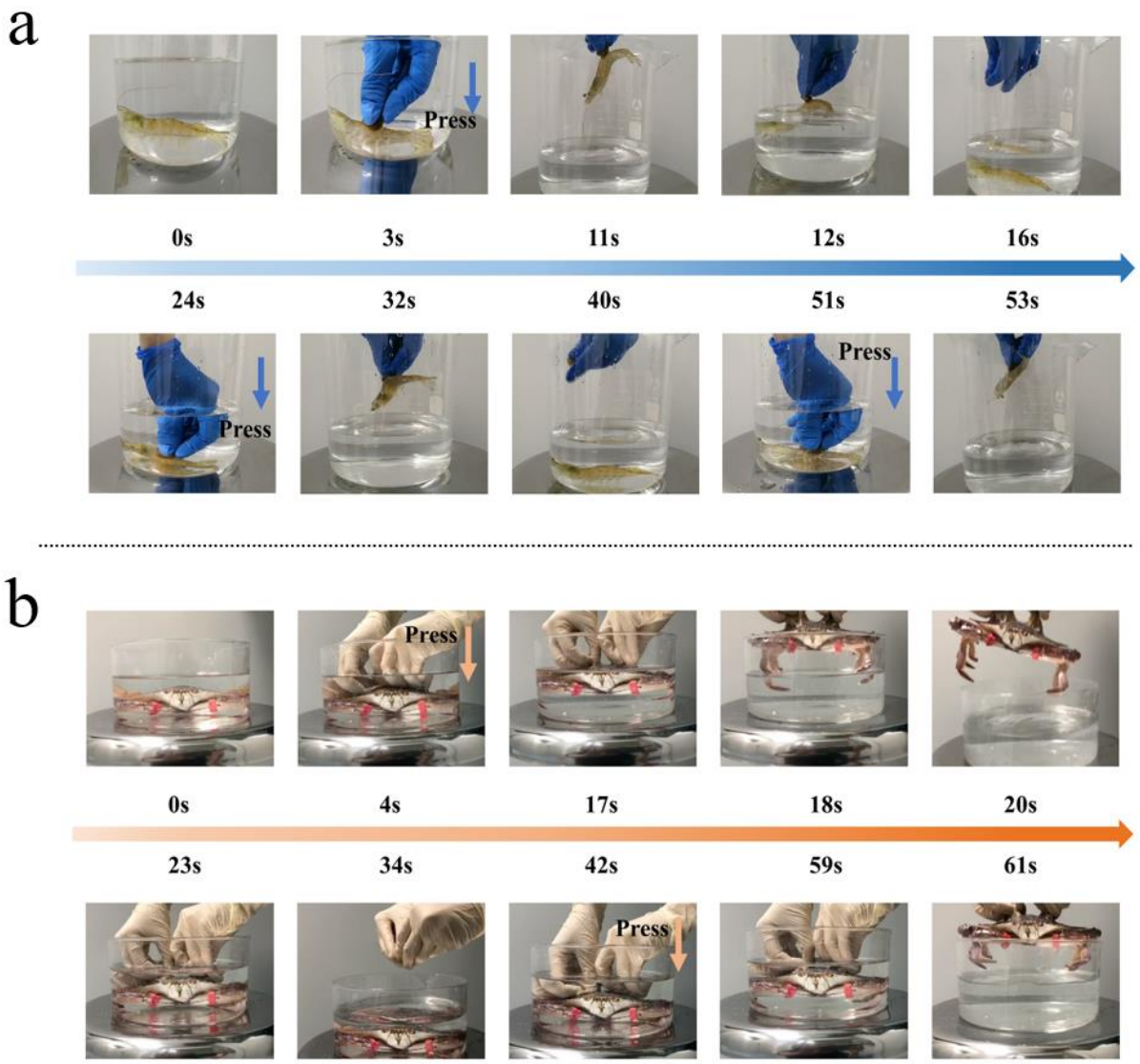

Fig. S23. Video screenshots of the efficient repeatable underwater adhesiveness of P-0.08Al-0.3T-0.3C to **a** a living shrimp and **b** a living crab. The underwater adhesiveness could be achieved simply by pressing the hydrogel on the back of a crustacean in several seconds. The hydrogel could be removed and adhere to the crustacean again in several seconds.

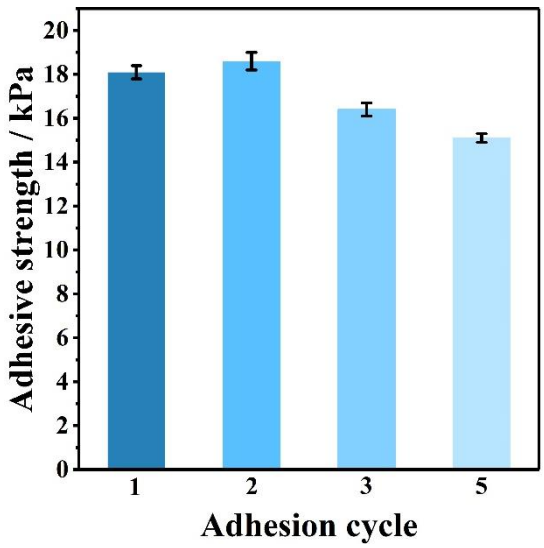

Fig. S24. Underwater adhesive strength of P-0.08Al-0.3C-0.3T to porcine skin after 1, 2, 3, or 5 times of adhesion (The samples were adhered, pressed for 10 sec in water and then tested immediately. In water, the adhered samples were peeled off and then adhered with the same piece of hydrogel again for multiple times).

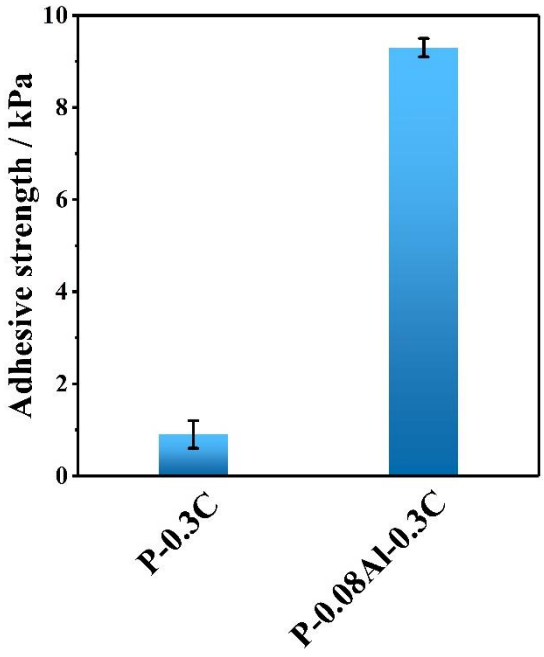

Fig. S25. Underwater adhesive strength to porcine skin of P-0.3C and P-0.08Al-0.3C with different contents of Al^{3+} (The samples were adhered, pressed for 10 sec in water and then tested immediately). Al^{3+} could effectively toughen the hydrogel network and thus affect the adhesiveness.[18]

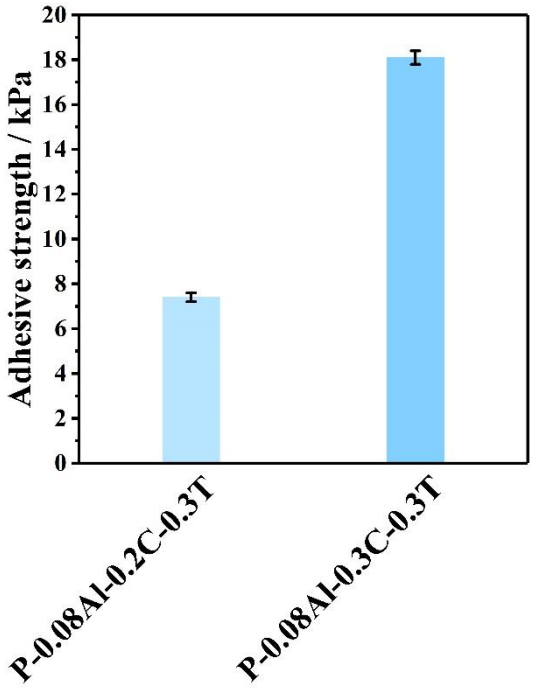

Fig. S26. Underwater adhesive strength to porcine skin of the hydrogels with different contents of CHI (The samples were adhered, pressed for 10 sec in water and then tested immediately). Higher amount of CHI provided more electrostatic bonding sites and improved the adhesive strength.[24, 27]

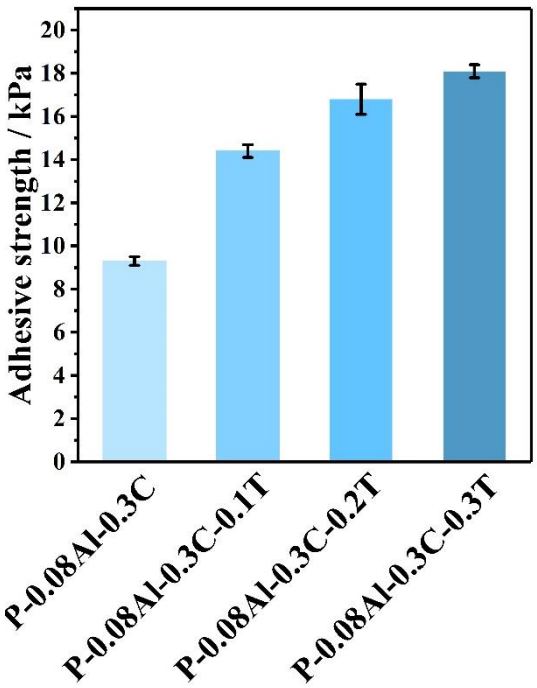

Fig. S27. Underwater adhesive strength to porcine skin of the hydrogels with different contents of TA (The samples were adhered, pressed for 10 sec in water and then tested immediately). Higher amount of TA provided more catechol groups and improved the adhesive strength.[5, 18]

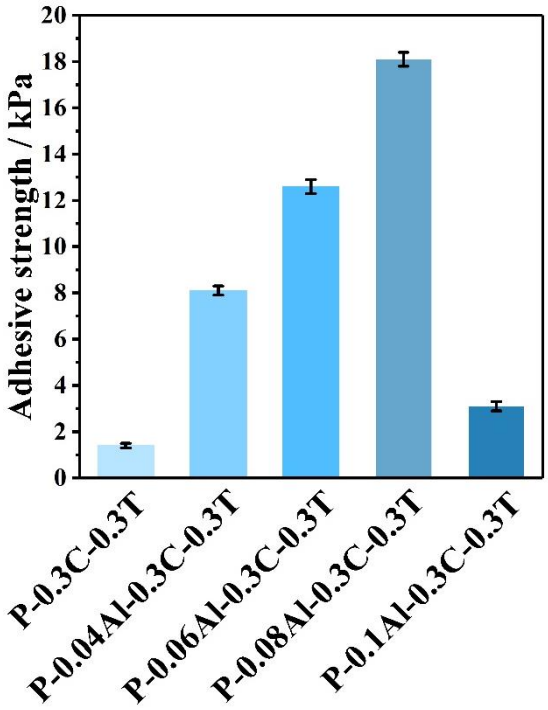

Fig. S28. Underwater adhesive strength to porcine skin of the hydrogels with different contents of Al^{3+} (The samples were adhered, pressed for 10 sec in water and then tested immediately). Al^{3+} could effectively toughen the hydrogel network and thus affect the adhesiveness.[18]

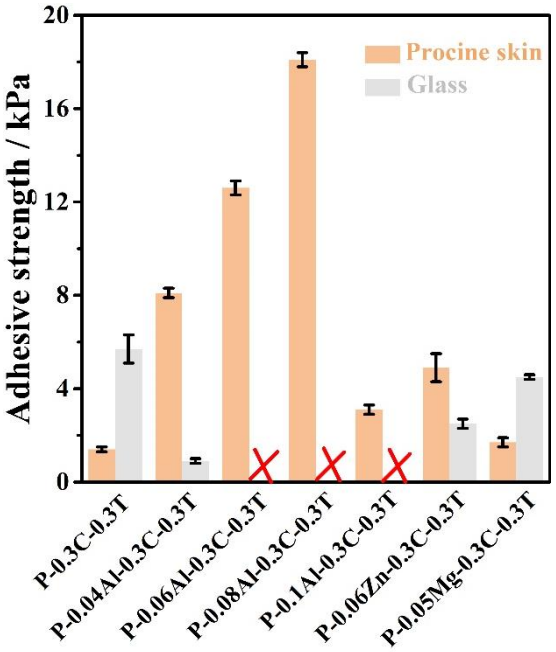

Fig. S29. Underwater adhesive strength to porcine skin or glass of the hydrogels containing Al^{3+}, Zn^{2+}, or Mg^{2+}. (The samples were adhered, pressed for 10 sec in water and then tested immediately. Red cross "×" meant this hydrogel was non-adhesive to underwater glass).

Considering the mechanical properties of the tested hydrogels, we found that Al^{3+} could better toughen the hydrogel network than Zn^{2+} or Mg^{2+}, and thus affect the adhesiveness.[18, 32, 33] The specificity of the underwater adhesion was closely related to the type and amount of metal ions because they had different influences on the underwater interfacial hydrogen bonding.[18, 20]

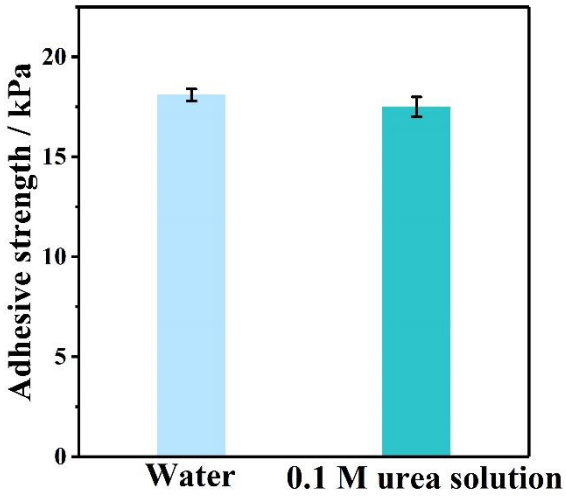

Fig. S30. Underwater adhesive strength of P-0.08Al-0.3C-0.3T to porcine skin in water or 0.1 M urea solution (The samples were adhered, pressed for 10 sec in water or 0.1 M urea solution and then tested immediately).

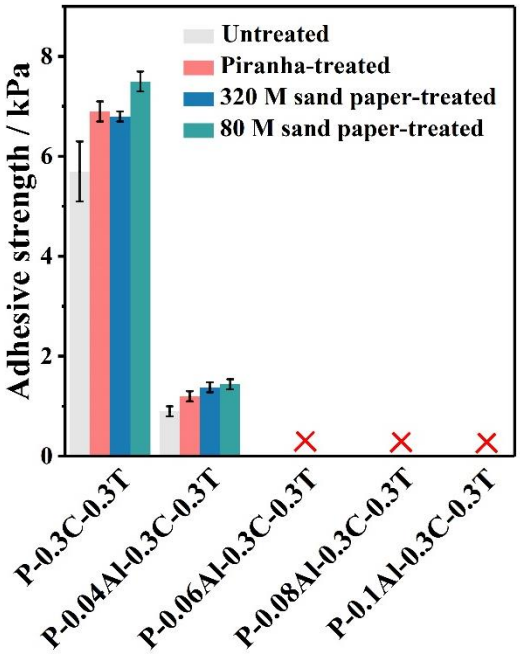

Fig. S31. Underwater adhesiveness of P-0.3C-0.3T, P-0.04Al-0.3C-0.3T, P-0.06Al-0.3C-0.3T, P-0.08Al-0.3C-0.3T and P-0.1Al-0.3C-0.3T to glass with different treatments (The

samples were adhered, pressed for 10 sec in water and then tested immediately. Red cross "×" meant this hydrogel was non-adhesive to underwater glass).

As for P-0.3C-0.3T and P-0.04Al-0.3C-0.3T, comparing the untreated and piranha-treated glass, the latter one tended to display higher underwater adhesive strength because of its increased surface hydroxyl groups.[3] Comparing the untreated glass with the glass treated with sand paper, the latter one display higher underwater adhesive strength. It was known that when the adhesive had good affinity with the adhered substrate, rough surface was beneficial for enhancing interfacial infiltration and adhesive strength.[34] However, as for P-0.06Al-0.3C-0.3T, P-0.08Al-0.3C-0.3T and P-0.1Al-0.3C-0.3T, no matter how the glass was treated, they showed no underwater adhesiveness (**Video S4**). This indicated the hydrogen bonding was effectively inhibited so that they displayed underwater specific adhesiveness.

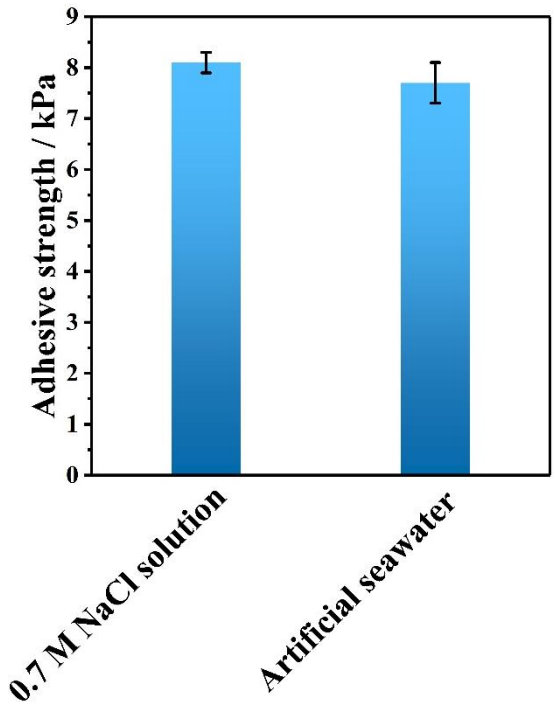

Fig. S32. Underwater adhesive strength of P-0.08Al-0.3C-0.3T to porcine skin in 0.7 M NaCl or artificial seawater (containing 0.7 M NaCl, 0.01 M KCl, 0.045 M $MgCl_2$ and 0.008 M $CaCl_2$)[35, 36] (The samples were adhered, pressed for 10 sec in 0.7 M NaCl solution or artificial seawater and then tested immediately).

In comparison with that in water, the decreased adhesive strength in the saline solution probably resulted from the Debye screening effect which could significantly impede the interfacial electrostatic bonding.[35, 37] K^+, Mg^{2+} and Ca^{2+} were at quite low concentration so the adhesive strength in artificial seawater was not significantly reduced comparing to that in 0.7 M NaCl.

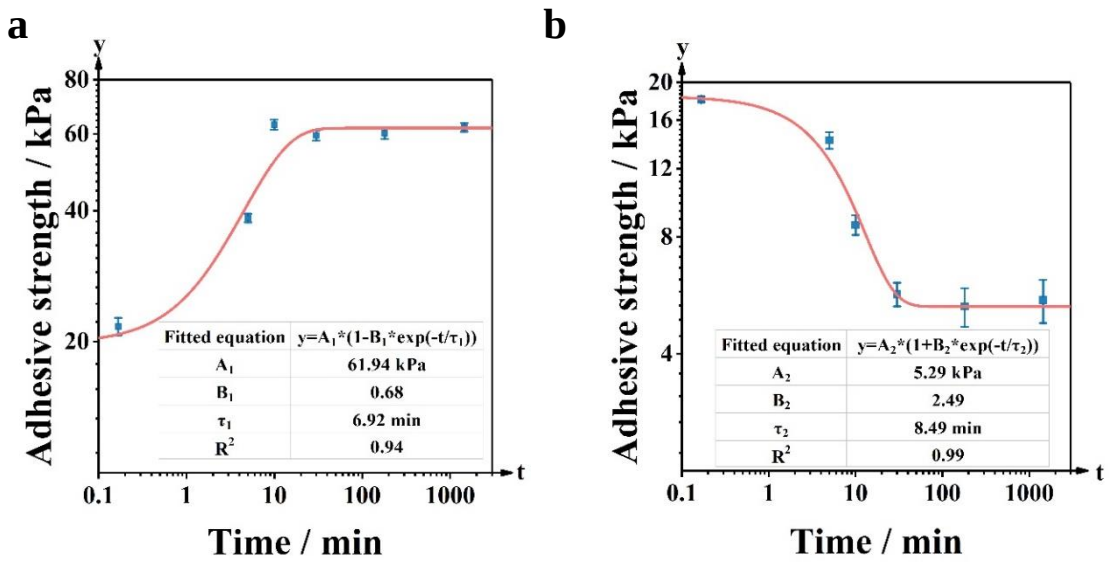

Fig. S33. Changes in adhesive strength to porcine skin **a** in air and **b** underwater with time. The statistical data (Mean±SD) denoted the experimental results, which were fitted with the expressions of $y = A_1 \times \left(1 - B_1 e^{-t/\tau_1}\right)$ and $y = A_2 \times \left(1 + B_2 e^{-t/\tau_2}\right)$, as shown in red solid curves, respectively. The values of the fitted parameters were presented in the figures, respectively. R^2 reached 0.94 and 0.99 in the fitting equations, respectively, implying that the curves could perfectly match the experimental data.

Based on the experimental data and the corresponding fitting curves, one could readily find that, in air, the adhesive strength to porcine skin gradually increased with time and eventually reached a plateau with a stable adhesive strength $A_1 = 61.94\ kPa$. The characteristic time scale τ_1 of the time-varying adhesive strength in air was $\tau_1 = 6.92\ min$, which meant that the adhesive strength on the time point of $t = 2\tau_1 \approx 14\ min$ had already been close to 90.8% of the stable strength (i.e., $1 - B_1 e^{-2} \approx 90.8\%$). In contrast, one could observe that the underwater adhesion strength of the hydrogels took on a gradually decreasing trend and also finally arrived at a stable equilibrium state, where the stable adhesive strength was $A_2 = 5.29\ kPa$ in water and the corresponding characteristic time scale was $\tau_2 = 8.49\ min$.

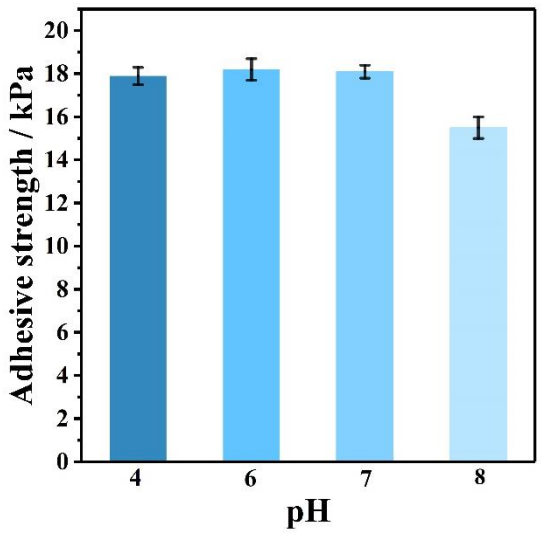

Fig. S34. Underwater adhesive strength of P-0.08Al-0.3C-0.3T adhering to porcine skin in water with different pH values (The samples were adhered, pressed for 10 sec in water with different pH values and then tested immediately).

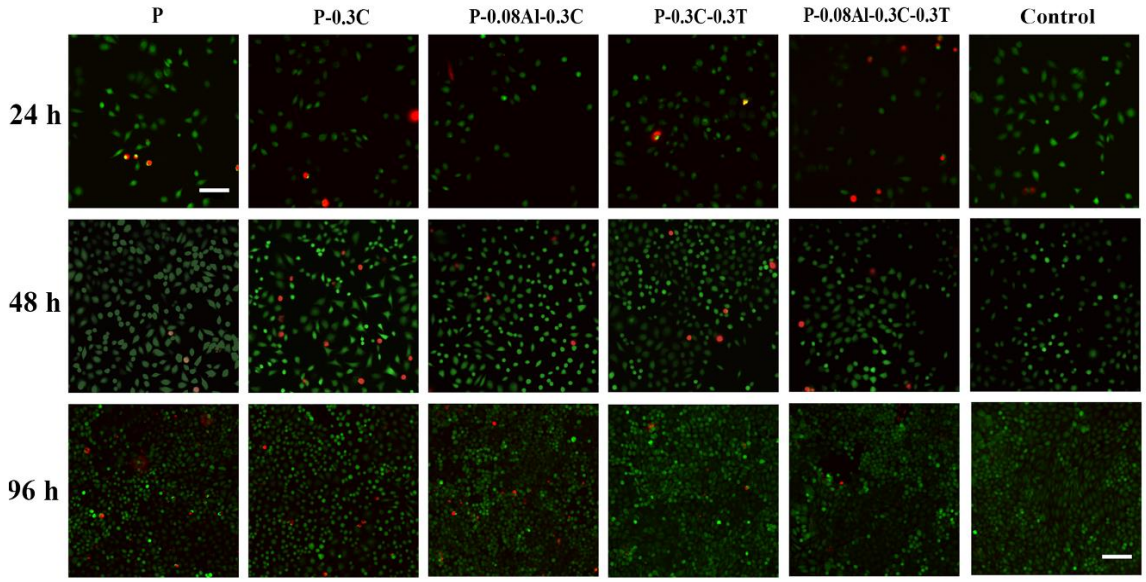

Fig. S35. Cytocompatibility of the P-0.08Al-0.3C-0.3T hydrogel and some other control samples. Confocal laser scanning microscopy (CLSM) graphs of fibroblasts in the extracts from the tested hydrogels.

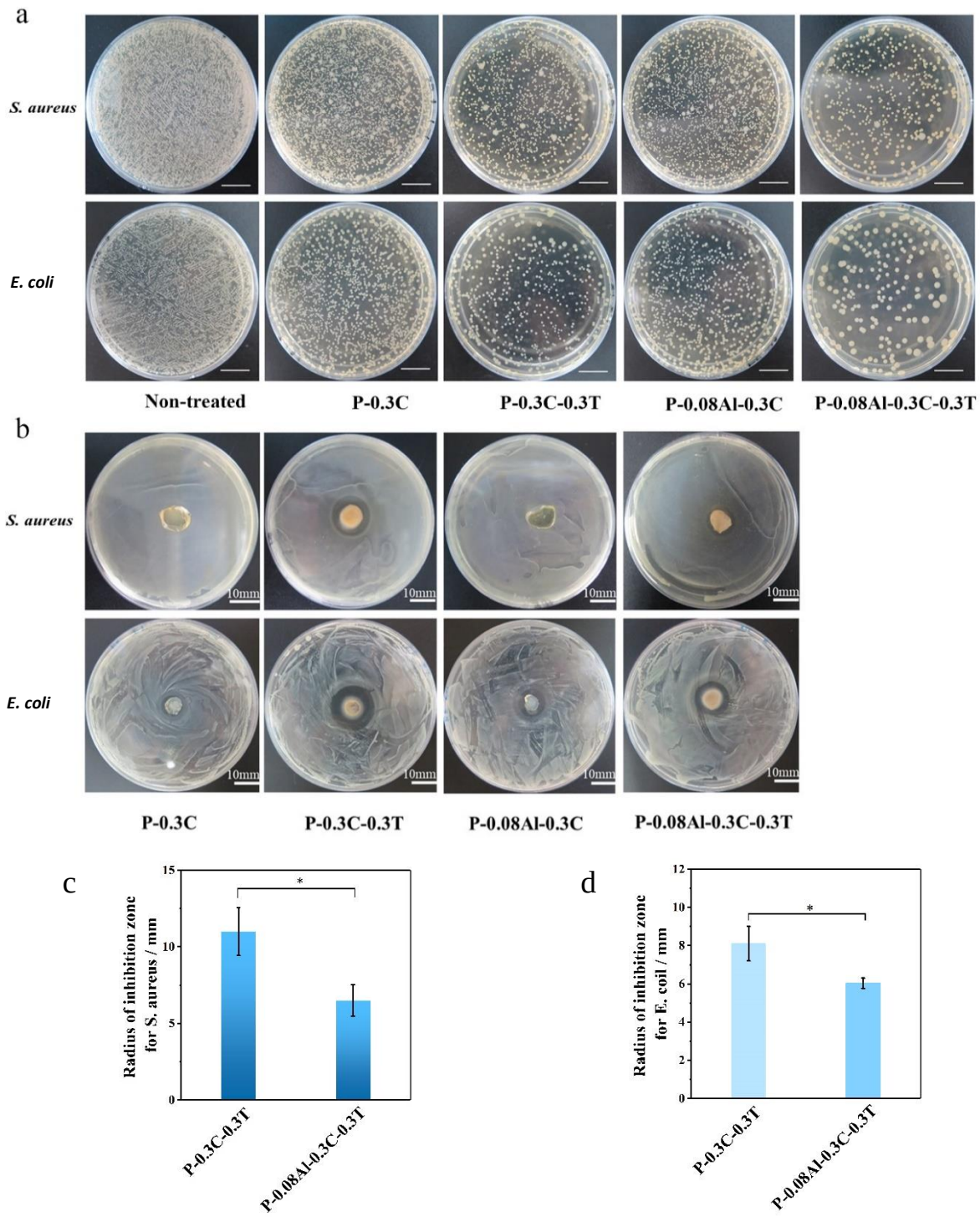

Fig. S36. Antibacterial properties of the hydrogels. **a** The tested hydrogels were co-cultured with *S. aureus* or *E. coli* with the density of 10^8 CFU/mL in Mueller-Hinton Broth medium for 24 hr, respectively. **b** The inhibitory zones of the tested hydrogels placed in the centre of Mueller-Hinton Agar (MHA) medium containing *S. aureus* or *E. coli* with the density of 10^6 CFU/mL. Statistic results were measured by Image J. for the radius of the inhibitory zones for **c** *S. aureus* or **d** *E. coli*. * indicate statistical difference at $p < 0.05$.

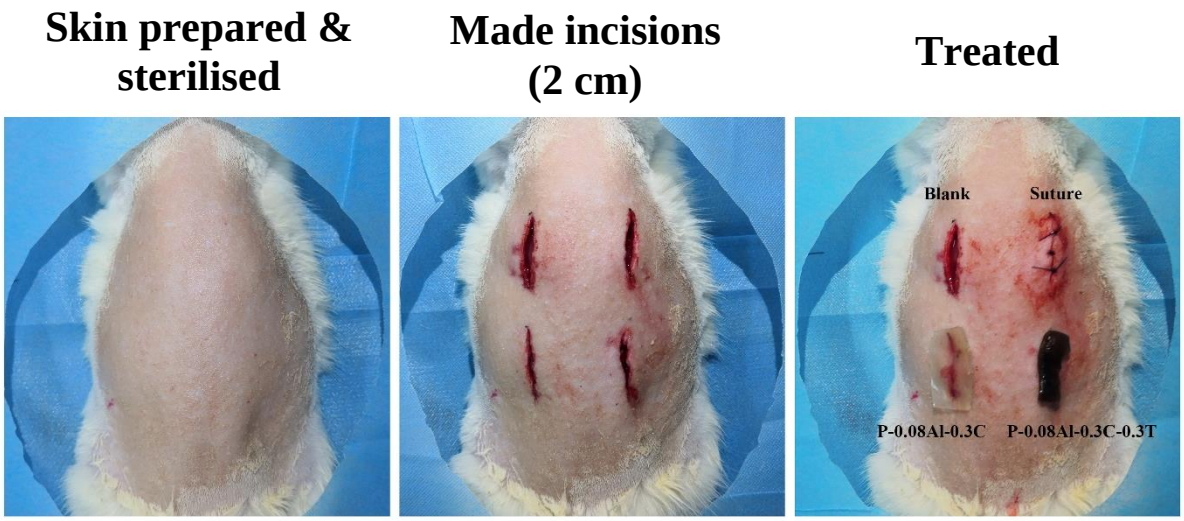

Fig. S37. Schematic illustration of the operations on the mouse back during wounding healing tests.

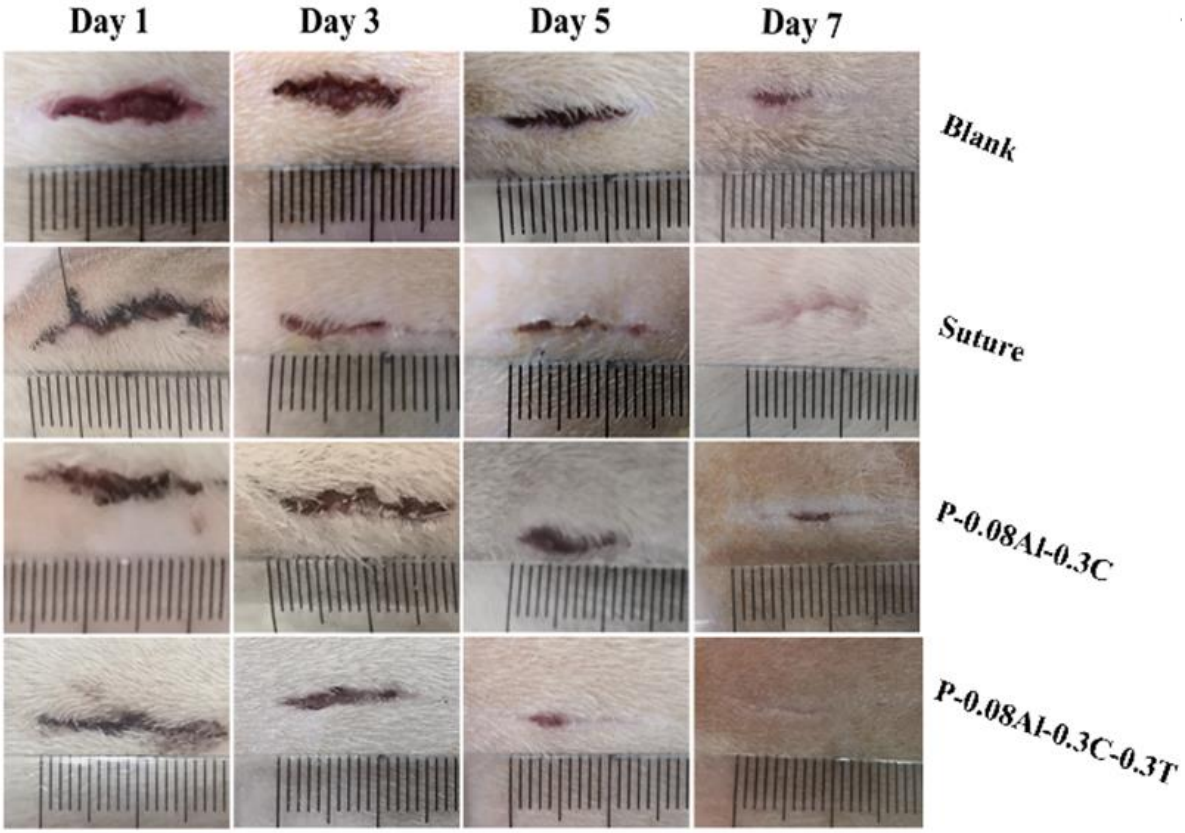

Fig. S38. The wound healing situation with different treatments at diverse time intervals.

Supplementary Tables

Table S1. Composition of the samples

Samples	AA (g)	BIS (mg)	APS (g)	$Al(NO_3)_3 \cdot 9H_2O$ (g)	CHI (g)	TA (g)	Deionized water (g)	Water content (wt. %)
P	3	10	0.08	0	0	0	10	77
P-0.08Al	3	10	0.08	0.08	0	0	10.3	77
P-0.3C	3	10	0.08	0	0.3	0	11	77
P-0.08Al-0.3C	3	10	0.08	0.08	0.3	0	11.3	77
P-0.3C-0.3T	3	10	0.08	0	0.3	0.3	12	77
P-0.08Al-0.3C-0.3T	3	10	0.08	0.08	0.3	0.3	12.3	77
P-0.08Al-0.3T	3	10	0.08	0.08	0	0.3	11.3	77
P-0.08Al-0.1C-0.3T	3	10	0.08	0.08	0.1	0.3	11.6	77
P-0.08Al-0.2C-0.3T	3	10	0.08	0.08	0.2	0.3	12	77
P-0.08Al-0.3C-0.1T	3	10	0.08	0.08	0.3	0.1	11.6	77
P-0.08Al-0.3C-0.2T	3	10	0.08	0.08	0.3	0.2	12	77
P-0.04Al-0.3C-0.3T	3	10	0.08	0.04	0.3	0.3	12.1	77
P-0.06Al-0.3C-0.3T	3	10	0.08	0.06	0.3	0.3	12.2	77
P-0.1Al-0.3C-0.3T	3	10	0.08	0.1	0.3	0.3	12.3	77
*P-0.08Al-0.3G-0.1T	3	10	0.08	0.08	0	0.1	11.6	77
*P-0.08Al-0.3G-0.3T	3	10	0.08	0.08	0	0.3	12.3	77
*P-0.08Al-0.3C-0.1D	3	10	0.08	0.08	0.3	0	11.6	77
*P-0.08Fe-0.3C-0.3T	3	10	0.08	0	0.3	0.3	12.3	77
*P-0.06Zn-0.3C-0.3T	3	10	0.08	0	0.3	0.3	12.3	77
*P-0.05Mg-0.3C-0.3T	3	10	0.08	0	0.3	0.3	12.3	77

*As for P-0.08Al-0.3G-0.1T and P-0.08Al-0.3G-0.3T, 0.3g guar gum (G) were used instead of 0.3g CHI. As for P-0.08Al-0.3C-0.1D, 0.1g dopamine (D) were used instead of 0.1g TA. 0.086g of $Fe(NO_3)_3 \cdot 9H_2O$, 0.063g of $Zn(NO_3)_2 \cdot 6H_2O$ or 0.055g of $Mg(NO_3)_2 \cdot 9H_2O$ was added instead of $Al(NO_3)_3 \cdot 9H_2O$, for synthesising P-0.08Fe-0.3C-0.3T, P-0.06Zn-0.3C-0.3T or P-0.05Mg-0.3C-0.3T, respectively. All the samples listed here were synthesised following the same methodology mentioned in the "**Synthesis of gels**" session.

Table S2. Comparison of properties for the existing adhesive hydrogels. (Note that the signs of '√', '×', and '-- ' denote 'Yes', 'No', and 'N/A', respectively)

Adhesive hydrogels	Time to achieve firm adhesion (substrate)	Adhesive strength test method	Adhesive strength in air (substrate)	Underwater Adhesive strength to soft bio-surfaces (substrate)	Underwater adhesive strength to Abiotic-surfaces (substrate)	Specific adhesion to bio-surfaces	Reversible adhesion in air	Reversible adhesion underwater	Self-healing In air (time)	Self-healing underwater (time)	Adhesive stability in acid or alkali
THIS WORK	10 sec (porcine skin)	Shear	63.3 kPa (fresh porcine skin)	18.1 kPa (fresh porcine skin)	×	√	√	√	√(30 sec)	√(30 sec)	√
Rao P, et al. Adv.Mater.2018[28]	10 sec (porcine pericardial)	Tensile	--	7 kPa (porcine pericardial)	25 kPa (glass)	--	√	√	--	--	--
Qiao H, et al. Acs Appl. Mater.Interfaces.2019[22]	-- (porcine skin)	Tensile	15 kPa (fresh porcine skin)	7 kPa (fresh porcine skin)	--	--	√	--	√(2 hr)	--	--
Cui CY, et al. Adv.Mater.2019[29]	10 sec (ceramic)	Shear	--	--	13 kPa (ceramic)	--	√	--	√	--	√
Han L, et al. Adv.Funct.Marer.2019[4]	120 sec (porcine skin)	Tensile	30 kPa (wet porcine skin after removing surface fat)	--	20 kPa (glass)	--	√	√	--	--	--
Fan HL, et al. Nat.Commun.2019[30]	10 sec (glass)	Tensile	--	--	60 kPa (glass)	--	--	√	--	--	√
Zhao YH, et al. Nat.Commun.2017[38]	-- (silicon)	Atomic Force Microscope	--	--	4 kPa (silicon)	--	√	--	--	--	--
Zhao Q, et al. Nat.Mater.2016[39]	10 min (glass)	Tensile	--	--	2 J/m^2 (glass)	--	--	--	--	--	--
Ju GN, et al. Angew.Chem.Int.Ed.2018[31]	5 min (PDDA)	Shear	--	--	6 kPa (PDDA)	--	√	--	--	--	--
Gao L, et al. Npg.Asia.Mate.2019[26]	4 hr (porcine skin)	Shear	55 kPa (fresh porcine skin)	--	--	--	√	--	--	--	--
Gan DL, et al. Nat.Commun.2019[40]	-- (porcine skin)	Tensile	30 kPa (fresh porcine skin)	--	--	--	√	--	--	--	--
Yuk H, et al. Nature.2019[41]	5 sec (porcine skin)	Shear	120 kPa (wet porcine skin) 160 kPa (fresh porcine skin)	--	--	--	--	--	--	--	--
Li J, et al. Science.2017[42]	3 min (porcine skin)	Peel	83 kPa (wet porcine skin)	--	--	--	--	--	--	--	--
Hong Y, et al. Nat.Commun.2019[43]	< 20 sec (porcine sausage skins)	Peel	80 kPa (wet sausage skin)	--	--	--	--	--	--	--	--
Han L, et al. ACS.Nano.2017[44]	-- (porcine skin)	Tensile	28.5 kPa (fresh porcine skin)	--	--	--	√	--	--	--	--
Han L, et al. Npg.Asia.Mate.2017[45]	-- (porcine skin)	Tensile	57 kPa (fresh porcine skin)	--	--	--	√	--	√	--	--
Rose S, et al. Nature.2014[46]	30 sec (calf liver)	Shear	25 J/ m^2 (fresh calf liver)	--	--	--	√	--	√	--	--
Lang N, et al. Sci.Transl.Med.2014[47]	5 sec (bovine pericardium)	Tensile	15 kPa (wet bovine pericardium) 20 kPa (fresh bovine pericardium)	--	--	--	--	--	--	--	--
Lang N, et al. Sci.Transl.Med.2014 (CA)[23]	5 sec (bovine pericardium)	Tensile	1 kPa (wet bovine pericardium) 38 kPa (fresh bovine pericardium)	--	--	--	--	--	--	--	--
Lang N, et al. Sci.Transl.Med.2014 (Fibrin sealant)[23]	5 sec (bovine pericardium)	Tensile	10 kPa (bovine amnion)	--	--	--	--	--	--	--	--
Yamagishi K, et al. Nat.Biom.Engine.2019[48]	30 min (muscle)	Tensile	0.507 J/m^2 (muscle)	--	--	--	√	--	--	--	--
Stapleton LM, et al. Nat.Biom.Engine.2019[49]	2min (sheep epicardial)	Tensile	1 kPa (sheep epicardial)	--	--	--	--	--	√	--	--
Chen HL, et al. Carbohydr.Polym.2018[25]	3 hr (porcine skin)	Shear	3 kPa (fresh porcine skin)	--	--	--	√	--	√(4 hr)	--	--
Li WX, et al. J.Mater.Chem.2018[23]	30 min (porcine skin)	Shear	6.26 kPa (fresh porcine skin)	--	--	--	√	--	√	--	--
Lih E, et al. Acta.Biomater.2012[24]	30 min (porcine skin)	Shear	97 kPa (fresh porcine skin)	--	--	--	√	--	√	--	--
Zhao X, et al. Biomaterials.2017[50]	3 hr (porcine skin)	Shear	4.9 kPa (fresh porcine skin)	--	--	--	--	--	√(2 hr)	--	--
Lin X, et al. Nat.Biom.Engine.2019[51]	-- (porcine epicardial)	Tensile	7 kPa (porcine epicardial)	--	--	--	--	--	--	--	--
Qu J, et al. Biomaterials.2018[52]	3 hr (porcine skin)	Shear	7 kPa (fresh porcine skin)	--	--	--	--	--	√	--	--

Table S3. The specificity of underwater adhesiveness for the tested hydrogels

Substrate / Hydrogel	Underwater, fresh, untreated porcine skin	Underwater, untreated glass	Underwater, piranha-treated glass	Underwater, 80 M sand paper-treated glass	Underwater, 320 M sand paper-treated glass
P	Non-adhesive	Non-adhesive	Non-adhesive	Non-adhesive	Non-adhesive
P-0.08Al	Non-adhesive	Non-adhesive	Non-adhesive	Non-adhesive	Non-adhesive
P-0.3C	Adhesive	Non-adhesive	Non-adhesive	Non-adhesive	Non-adhesive
P-0.3C-0.3T	Adhesive	Adhesive	Adhesive	Adhesive	Adhesive
P-0.08Al-0.3C	Adhesive	Non-adhesive	Non-adhesive	Non-adhesive	Non-adhesive
P-0.08Al-0.2C-0.3T	Adhesive	Non-adhesive	Non-adhesive	Non-adhesive	Non-adhesive
P-0.04Al-0.3C-0.3T	Adhesive	Adhesive	Adhesive	Adhesive	Adhesive
P-0.06Al-0.3C-0.3T	Adhesive	Non-adhesive	Non-adhesive	Non-adhesive	Non-adhesive
P-0.08Al-0.3C-0.3T	Adhesive	Non-adhesive	Non-adhesive	Non-adhesive	Non-adhesive
P-0.1Al-0.3C-0.3T	Adhesive	Non-adhesive	Non-adhesive	Non-adhesive	Non-adhesive
P-0.08Al-0.3G-0.1T	Adhesive	Adhesive	Adhesive	Adhesive	Adhesive
P-0.06Zn-0.3C-0.3T	Adhesive	Adhesive	Adhesive	Adhesive	Adhesive
P-0.05Mg-0.3C-0.3T	Adhesive	Adhesive	Adhesive	Adhesive	Adhesive

Table S4. Swelling ratios (SR)* of hydrogels at room temperature

Hydrogels	**SR for the as-prepared hydrogels**	**SR in water for two weeks**	**SR in PBS for two weeks**
P	3.35	240.9 ± 32.6	57.1 ± 8.6
P-0.08Al	3.35	37.3 ± 3.3	26.6 ± 1.3
P-0.3C	3.35	18.8 ± 0.6	20.6 ± 2.1
P-0.08Al-0.3C	3.35	16.7 ± 0.5	16.3 ± 1.3
P-0.3C-0.3T	3.35	26.6 ± 2.6	10.1 ± 1.5
P-0.08Al-0.3C-0.3TA	3.35	12.5 ± 0.5	5.3 ± 0.3
P-0.06Zn-0.3C-0.3T	3.35	14.0 ± 0.5	6.6 ± 0.2
P-0.05Mg-0.3C-0.3T	3.35	22.9 ± 1.6	8.8 ± 0.3

Supplementary Videos

Video S1: The mechanical performance of P-0.08Al-0.3C-0.3T when stretched.

Video S2: The mechanical performance of P-0.08Al-0.3C-0.3T when compressed.

Video S3: The self-healing ability of P-0.08Al-0.3C-0.3T.

Video S4: The non-adhesive property of P-0.08Al-0.3C-0.3T to underwater glass in contrast to P-0.06Zn-0.3C-0.3T.

Video S5: The efficient underwater adhesiveness of P-0.08Al-0.3C-0.3T to porcine skin.

Video S6: The reversible and efficient underwater adhesiveness of P-0.08Al-0.3C-0.3T to a living shrimp.

Video S7: The reversible and efficient underwater adhesiveness of P-0.08Al-0.3C-0.3T to a living crab.

References

1. X. Su and B. Chen, *Carbohydr. Polym.*, 2018, **197**, 497-507.
2. D. Gan, W. Xing, L. Jiang, J. Fang, C. Zhao, F. Ren, L. Fang, K. Wang and X. Lu, *Nat. Commun.*, 2019, **10**, 1487.
3. J. Canning, I. Petermann and K. Cook, *Proceedings of SPIE the International Society for Optical Engineering*, 2012, **8351**, 89.
4. L. Han, M. Wang, L. O. Prieto-López, X. Deng and J. Cui, *Adv. Funct. Mater.*, 2020, **30**, 1907064.
5. L. Han, L. W. Yan, K. F. Wang, L. M. Fang, H. P. Zhang, Y. H. Tang, Y. H. Ding, L. T. Weng, J. L. Xu, J. Weng, Y. J. Liu, F. Z. Ren and X. Lu, *NPG Asia Mater.*, 2017, **9**, 12.
6. C. Y. Gao, Z. H. Huang, W. Jing, P. F. Wei, L. Jin, X. H. Zhang, Q. Cai, X. L. Deng and X. P. Yang, *J. Mater. Chem. B*, 2018, **6**, 7471-7485.
7. Z. Yuan, P. Wei, Y. Huang, W. Zhang, F. Chen, X. Zhang, J. Mao, D. Chen, Q. Cai and X. Yang, *Acta biomaterialia*, 2019, **85**, 294-309.
8. V. Rubentheren, T. A. Ward, C. Y. Chee, P. Nair, E. Salami and C. Fearday, *Carbohydr. Polym.*, 2016, **140**, 202-208.
9. S. Rivero, M. A. García and A. Pinotti, *Carbohydr. Polym.*, 2010, **82**, 270-276.
10. K. Driver, S. Baco and V. V. Khutoryanskiy, *Eur. Polym. J.*, 2013, **49**, 4249-4256.
11. H. Zhu, Z. Chen, S. Yong and T. T. L. Thi, *Dyes & Pigments*, 2010, **86**, 155-160.
12. V. Chavasit, C. Kienzle-Sterzer and J. A. Torres, *Polym. Bull.*, 1988, **19**, 223-230.
13. X. Hou, F. Fang, X. Guo, J. Wizi, B. Ma, Y. Tao and Y. Yang, *ACS Sustain. Chem. Eng.*, 2017, **5**, 4589-4597.
14. Y. Z. Piao and B. Q. Chen, *RSC Adv.*, 2016, **6**, 6171-6181.
15. X. Su, S. Mahalingam, M. Edirisinghe and B. Chen, *ACS Appl. Mater. Interfaces*, 2017, **9**, 22223-22234.
16. K. Yu, D. Wong, J. Parasrampuria and D. Friend, 1996, **24**, 243-276.
17. K. Schoellkopf, R. Albrecht, M. Lehmann and G. Schroeder, 1990.
18. C. Shao, M. Wang, L. Meng, H. Chang, B. Wang, F. Xu, J. Yang and P. Wan, *Chem. Mater.*, 2018, **30**, 3110-3121.
19. J. Y. Sun, X. H. Zhao, W. R. K. Illeperuma, O. Chaudhuri, K. H. Oh, D. J. Mooney, J. J. Vlassak and Z. G. Suo, *Nature*, 2012, **489**, 133-136.
20. X. H. Wang, F. Song, D. Qian, Y. D. He, W. C. Nie, X. L. Wang and Y. Z. Wang, *Chem. Eng. J.*, 2018, **349**, 588-594.
21. J. Pan, Y. Jin, S. Lai, L. Shi, W. Fan and Y. Shen, *Chem. Eng. J.*, 2019, **370**, 1228-1238.
22. H. Qiao, P. Qi, X. Zhang, L. Wang, Y. Tan, Z. Luan, Y. Xia, Y. Li and K. Sui, *ACS Appl. Mater. Interfaces*, 2019, **11**, 7755-7763.
23. W. X. Li, R. Y. Feng, R. S. Wang, D. Li, W. W. Jiang, H. Z. Liu, Z. Z. Guo, M. J. Serpe and L. Hu, *J. Mater. Chem. B*, 2018, **6**, 4799-4807.
24. E. Lih, J. S. Lee, K. M. Park and K. D. Park, *Acta Biomaterialia*, 2012, **8**, 3261-3269.
25. H. L. Chen, J. W. Cheng, L. X. Ran, K. Yu, B. T. Lu, G. Q. Lan, F. Y. Dai and F. Lu, *Carbohydr. Polym.*, 2018, **201**, 522-531.
26. L. Gao, Y. Zhou, J. Peng, C. Xu, Q. Xu, M. Xing and J. Chang, *NPG Asia Mater.*, 2019, **11**, 66.
27. B. Balakrishnan, D. Soman, U. Payanam, A. Laurent, D. Labarre and A. Jayakrishnan, *Acta Biomaterialia*, 2017, **53**, 343-354.
28. P. Rao, T. L. Sun, L. Chen, R. Takahashi, G. Shinohara, H. Guo, D. R. King, T. Kurokawa and J. P. Gong, *Adv. Mater.*, 2018, **30**, 1801884.
29. C. Y. Cui, C. C. Fan, Y. H. Wu, M. Xiao, T. L. Wu, D. F. Zhang, X. Y. Chen, B. Liu, Z. Y. Xu, B. Qu and W. G. Liu, *Adv. Mater.*, 2019, **31**, 1905761.

30. H. L. Fan, J. H. Wang, Z. Tao, J. C. Huang, P. Rao, T. Kurokawa and J. P. Gong, *Nat. Commun.*, 2019, **10**, 5127.
31. G. N. Ju, M. J. Cheng, F. L. Guo, Q. Zhang and F. Shi, *Angew. Chem. Int. Ed.*, 2018, **57**, 8963-8967.
32. X. Liu, Z. Chen, L. Wang and J. Shen, *Chem. Eng. J.*, 2012, **211-212**, 179-185.
33. R. Roma-Luciow, L. Sarraf and M. Morcellet, *Eur. Polym. J.*, 2001, **37**, 1741-1745.
34. P. H. Frota, A. D. Loguercio, A. Reis and J. Bauer, IADR General Session, 2012.
35. H. Fan, J. Wang, Z. Tao, J. Huang, P. Rao, T. Kurokawa and J. P. Gong, *Nat. Commun.*, 2019, **10**, 5127.
36. K. Kang, P. Linga, K. N. Park, S. J. Choi and J. D. Lee, *Desalination*, 2014, **353**, 84-90.
37. J. N. Israelachvili, *Q. Rev. Biol.*, 2011, **2**, 59–65.
38. Y. H. Zhao, Y. Wu, L. Wang, M. M. Zhang, X. Chen, M. J. Liu, J. Fan, J. Q. Liu, F. Zhou and Z. K. Wang, *Nat. Commun.*, 2017, **8**, 2218.
39. Q. Zhao, D. W. Lee, B. K. Ahn, S. Seo, Y. Kaufman, J. N. Israelachvili and J. H. Waite, *Nat. Mater.*, 2016, **15**, 407-412.
40. D. L. Gan, W. S. Xing, L. L. Jiang, J. Fang, C. C. Zhao, F. Z. Ren, L. M. Fang, K. F. Wang and X. Lu, *Nat. Commun.*, 2019, **10**, 1487.
41. H. Yuk, C. E. Varela, C. S. Nabzdyk, X. Mao, R. F. Padera, E. T. Roche and X. Zhao, *Nature*, 2019, **575**, 169-174.
42. J. Li, A. D. Celiz, J. Yang, Q. Yang, I. Wamala, W. Whyte, B. R. Seo, N. V. Vasilyev, J. J. Vlassak, Z. Suo and D. J. Mooney, *Science*, 2017, **357**, 378-381.
43. Y. Hong, F. F. Zhou, Y. J. Hua, X. Z. Zhang, C. Y. Ni, D. H. Pan, Y. Q. Zhang, D. M. Jiang, L. Yang, Q. N. Lin, Y. W. Zou, D. S. Yu, D. E. Arnot, X. H. Zou, L. Y. Zhu, S. F. Zhang and H. W. Ouyang, *Nat. Commun.*, 2019, **10**, 2060.
44. L. Han, X. Lu, K. Z. Liu, K. F. Wang, L. M. Fang, L. T. Weng, H. P. Zhang, Y. H. Tang, F. Z. Ren, C. C. Zhao, G. X. Sun, R. Liang and Z. J. Li, *ACS Nano*, 2017, **11**, 2561-2574.
45. L. Han, L. W. Yan, K. F. Wang, L. M. Fang, H. P. Zhang, Y. H. Tang, Y. H. Ding, L. T. Weng, J. L. Xu, J. Weng, Y. J. Liu, F. Z. Ren and X. Lu, *Npg Asia Mater.*, 2017, **9**, 372.
46. S. Rose, A. Prevoteau, P. Elziere, D. Hourdet, A. Marcellan and L. Leibler, *Nature*, 2014, **505**, 382-385.
47. N. Lang, M. J. Pereira, Y. Lee, I. Friehs, N. V. Vasilyev, E. N. Feins, K. Ablasser, E. D. O'Cearbhaill, C. J. Xu, A. Fabozzo, R. Padera, S. Wasserman, F. Freudenthal, L. S. Ferreira, R. Langer, J. M. Karp and P. J. del Nido, *Science Translational Medicine*, 2014, **6**, 218.
48. K. Yamagishi, I. Kirino, I. Takahashi, H. Amano, S. Takeoka, Y. Morimoto and T. Fujie, *Nat. Biomed. Eng.*, 2019, **3**, 27-36.
49. L. M. Stapleton, A. N. Steele, H. Wang, H. L. Hernandez, A. C. Yu, M. J. Paulsen, A. A. A. Smith, G. A. Roth, A. D. Thakore, H. J. Lucian, K. P. Totherow, S. W. Baker, Y. Tadas, J. M. Farry, A. Eskandari, C. E. Hironaka, K. J. Jaatinen, K. M. Williams, H. Bergamasco, C. Marschel, B. Chadwick, F. Grady, M. Mae, E. A. Appel and Y. J. Woo, *Nat. Biomed. Eng.*, 2019, **3**, 611-620.
50. X. Zhao, H. Wu, B. L. Guo, R. N. Dong, Y. S. Qiu and P. X. Ma, *Biomaterials*, 2017, **122**, 34-47.
51. X. Lin, Y. Liu, A. Bai, H. Cai, Y. Bai, W. Jiang, H. Yang, X. Wang, L. Yang, N. Sun and H. Gao, *Nat. Biomed. Eng.*, 2019, **3**, 632-643.
52. J. Qu, X. Zhao, Y. P. Liang, T. L. Zhang, P. X. Ma and B. L. Guo, *Biomaterials*, 2018, **183**, 185-199.